Ref. Ares(2025)3493315 - 30/04/2025

RadoNorm
Managing risks from radon and NORM

Deliverable 2.10

Review of existing studies on radon in underground voids and possible correlation with indoor radon and results of the correlation study between voids and indoor/in soil radon based on data from partners and new measurements

Work Package 2

Mario Caprio, Francesco Bochicchio, Sebastian Baumann,
Ivana Fojtikova, Joëlle Goyette Pernot, Claire Greau, Valeria Gruber,
Nahla Mansouri, Joan Frédéric Rey, Trilochana Shetty.

This project has received funding from the Euratom research and training programme 2019-2020 under grant agreement No 900009.

Document information

Project Acronym	**RadoNorm**
Project Title	**Towards effective radiation protection based on improved scientific evidence and social considerations - focus on radon and NORM**
Project Type	**RIA**
EC grant agreement No.	**900009**
Project starting / end date	**1st September 2020 – 31 August 2025**
Work Package No.	**2**
Work Package Title	**Exposure**
Deliverable No.	**2.10**
Deliverable Title	**Review of existing studies on radon in underground voids and possible correlation with indoor radon and results of the correlation study between voids and indoor/in soil radon based on data from partners and new measurements**
Lead Beneficiary	**ISS**
Contractual Delivery Date	**30.04.2025**
Actual Delivery Date	**30.04.2025**
Type	**Report**
Dissemination level	**Public**
Authors	**ISS, AGES, HES-SO, ASNR, SURO**

To be cited as:

Caprio M., Bochicchio F., Baumann S., Fojtikova I., Goyette Pernot J., Greau C., Gruber V., Mansouri N., Rey J. F., Shetty T. (2025): Review of existing studies on radon in underground voids and possible correlation with indoor radon and results of the correlation study between voids and indoor/in soil radon based on data from partners and new measurements. Final version as of 30.04.2025 of deliverable D2.10 of project RadoNorm

Disclaimer

This document reflects only the author's view and the European Commission is not responsible for any use that may be made of the information it contains.

Acknowledgement

This document is a deliverable of the RadoNorm project. This project has received funding from the Euratom research and training programme 2019-2020 under grant agreement No 900009.

Status of deliverable		
	By	Date
Delivered (Lead Beneficiary)	M. Caprio	23.04.2025
Verified (WP Leader)	Laureline Février	25.04.2025
Reviewed (Reviewers)	WPL, PC	29.04.2025
Approved	PC	30.04.2025
Submitted to EC	PC	30.04.2025

Executive Summary

Within the European RadoNorm project, work package 2 aimed at providing a better characterisation of exposures of humans to ionising radiation, and Task 2.4, entitled "*Improvement of methods to identify high indoor Rn levels (Rn mapping and other methods)"* focuses, in particular, on high radon concentrations. The present report is the milestone MS21 and is part of subtask 2.4.2, entitled "*Studying the influence of local underground voids, both of karstic and anthropic (e.g., caves and catacombs) origins, on radon levels*".

This report consists of two main parts. The first part is dedicated to the bibliography review. The review aims at collecting literature in which there is evidence of both correlations between voids and radon concentration measurements in dwellings above the voids and characterization of different types of voids in terms of radon concentration.

The second part of this report is focused on describing suitable datasets to perform two different types of analyses. One analysis deals with the eventual correlation between voids and radon concentration in dwellings above the voids and the other with the evaluation of radon concentration values in different types of voids.

Table of contents

List of Tables

List of figures

Introduction

In the European RadoNorm project, Work Package 2 is focused on the characterisation of exposures to ionising radiation. The subtask 2.4.2 entitled "*Studying the influence of local underground voids, both of karstic and anthropic (e.g., caves and catacombs) origins, on radon levels*" aims in particular to study correlations between voids and radon concentrations in dwellings above voids.

The first part is dedicated to a bibliography review, which aims at collecting literature in which there is evidence of both correlations between voids and radon concentration measurements in dwellings above the voids and characterisation of different types of voids in terms of radon concentration.

The second part of the report is focused on describing suitable datasets to perform two different types of analyses. One type of the analysis deals with the eventual correlation between voids and radon concentration in dwellings above the voids and the other with the evaluation of radon concentration values in different types of voids.

1 Bibliographic Review

1.1 Introduction

This bibliography review aims at collecting literature with the evidence of correlation between voids and radon concentration measurements in dwellings above the voids, as well as published studies in order to characterise different types of voids in terms of radon concentration.

For this purpose, bibliography research has been done in three different databases: PubMed, Scopus and Web of Science. The results of this search, a list of scientific publications, have been evaluated among partners to select those matching our constraints.

1.2 Methods

A literature search has been performed, for both "Correlation between voids and radon concentration measurements in dwellings above the voids" and "Radon concentration measurements in different types of voids ", by queries with fields of interest described hereafter:

{field} -> Title/Abstract, Keywords

{timespan} -> All

{language} -> All languages

{databases} -> Scopus, Web of Science, PubMed

{search engine} -> Google Scholar (to be used to integrate/refine the lit search performed through the 3 main databases cited above)

{Information sources} -> peer-reviewed journals, conference proceedings, reports of international organisations, and governmental reports.

The details of the two queries used for the bibliography search are:

- **Query 1** on "Identify studies on the influence of underground voids on radon level in dwelling located above voids" a described in Table 1.

- **Query 2** on "Identify studies on the radon concentration values inside different type of voids." as described in Table 2.

The syntax used to perform the two queries in the three different databases (**PubMed**, **Scopus** and **Web of Science**) are reported in Table 3.

*Table 1 – Query 1 (*Identify studies on the influence of underground voids on radon level in dwellings located above voids.*)*

radon **OR** *Rn-222* **OR** *222Rn* **OR** *(222)Rn*	**AND**	*Void** **OR** *Tunnel** **OR** *Catacomb** **OR** *Bunker** **OR** *Cavit** **OR** *karst** **OR** *"underground spaces"* **OR** *"underground hollows*	**AND**	*Dwelling** **OR** *Room** **OR** *Building** **OR** *Workplace** **OR** *School**

Table 2 - Query 2 (*Identify studies on the radon concentration values inside different type of voids)*

radon **OR** *Rn-222* **OR** *222Rn* **OR** *(222)Rn*	**AND**	*subway* **OR** *railway* **OR** *metro* **OR** *"metro station"* **OR** *"underground metro"*

Table 3 – Syntax used for each query and for each Database.

DB	Query n.	Query (syntax)	Results (N.)
PubMed	1	(radon[Title/Abstract] OR “Rn”[Title/Abstract] OR Rn-222[Title/Abstract] OR 222Rn[Title/Abstract]) AND (void*[Title/Abstract] OR Tunnel*[Title/Abstract] OR Catacomb*[Title/Abstract] OR Bunker*[Title/Abstract] OR Cavit*[Title/Abstract] OR Karst*[Title/Abstract] OR “underground spaces”[Title/Abstract] OR “underground hollows” [Title/Abstract]) AND (dwelling*[Title/Abstract] OR Room*[Title/Abstract] OR Building*[Title/Abstract] OR Workplace*[Title/Abstract])	34
	2	(radon[Title/Abstract] OR “Rn”[Title/Abstract] OR Rn-222[Title/Abstract] OR 222Rn[Title/Abstract]) AND (subway[Title] OR railway[Title] OR metro[Title] OR “metro station”[Title] OR “underground metro”[Title])	10
WoS	1	TI=(radon OR "Rn" OR Rn-222 OR 222Rn) AND TS = (void* OR Tunnel* OR Catacomb* OR Bunker* OR Cavit* OR Karst* OR "underground spaces" OR "underground hollows") AND TS = (dwelling* OR Room* OR Building* OR Workplace*)	50
	2	TI=(radon OR “Rn” OR Rn-222 OR 222Rn) AND TI=(subway OR railway OR metro OR “metro station” OR “underground metro”)	17
Scopus	1	TITLE(radon OR “(222)Rn” OR 222Rn OR “Rn-222”) AND TITLE-ABS(void* OR Tunnel* OR catacomb OR Bunker* OR cavit* OR karst* OR “underground spaces” OR “underground hollows”) AND TITLE-ABS(dwelling* OR room* OR building* OR workplace* OR school*)	79
	2	TITLE(radon OR “(222)Rn” OR 222Rn OR Rn-222) AND TITLE-ABS (subway OR railway OR metro OR “metro station” OR “underground metro”)	39

The bibliography search (performed on 10/11/2022) returned 229 papers, for the two queries together, respectively 163 scientific publications (Query 1) and 66 scientific publications (Query 2). The number of papers found are reported in the last column of the Table 3.

Duplicated papers in the three different databases are removed from search results and the details are reported in Table 4 and Table 5. So, we focused on 130 papers to evaluate (93 from Query 1 and 37 from Query 2).

Table 4 – Summary result of Query 1.

Date	DB	Results	Results (without duplicates)
10/11/2022	PubMed	34	28
10/11/2022	WoS	50	15
10/11/2022	Scopus	79	50
	TOT	**163**	**93**

Table 5 - Summary result of Query 2.

Date	DB	Results	Results (without duplicates)
10/11/2022	PubMed	10	10
10/11/2022	WoS	17	2
10/11/2022	Scopus	39	25
	TOT	**66**	**37**

1.3 Paper's evaluation process

Information about each paper was collected using an Excel spreadsheet to identify the papers selected from the bibliography search and to record the selection/rejection criteria.

The evaluation process is developed in two steps. In the first one (**pre-selection**) the papers were selected by reading only the abstract. In this step all papers that matched our aims, i.e. papers that deal with the correlation of radon measurements in dwellings above voids or the radon measurements in voids of different types, were selected. In the second step (IARC, #1275), the papers were evaluated in detail by full text reading.

Pre-selection of papers

The 130 papers (93 from Query 1 and 37 from Query 2) retrieved from the bibliography search have been distributed among partners to pre-select them.

Papers attained to the correlation between voids and radon concentration above voids and radon concentration in voids of different types have been evaluated and the results reported in an Excel file containing the following fields (Table 6):

Table 6 – Main Information fields to retrieve, in the pre-selection step.

FIELDS
Authors
Year
Title
Abstract
Journal
Useful for the review (yes/no)
Reason for selecting
Reason for rejecting
Assessor

The output of the pre-selection led to 46 papers of which 26 were from Query 1 and 20 from Query 2. The excluded 84 papers, 67 from Query 1 and 17 from Query 2, are not of interest for our review.

Evaluation of papers

For all papers from the pre-selection step (46, 26 from Query 1 and 20 from Query 2), a search has been done to retrieve them in PDF format. This work reduced the number of papers to 39.

Five of the 39 papers, that seemed interesting in the pre-selection step, have been discarded subsequently after reading the full text (they did not fit with our purposes).

In addition, we also considered 3 papers [2, 14, 34] with very useful information (by abstract) for our review although without a full text available. So, our review will be based on a total of **37** papers.

All papers have been evaluated in detail and, to make the process easier, a datasheet in Excel format has been prepared in order to select, from all papers, the key information as reported in Table 7. All these fields were aimed to focus on the main characteristics of the voids.

Table 7 – Main Information key to retrieve from papers.

FIELDS
Who evaluates
Review
Type of void
Void's extension (depth, length, width)
Ventilated Void? (Yes/No)
In case of ventilated voids, natural or artificial ventilation?
Are there measurements of Rn concentration for voids?
How many measurements of radon concentration in voids
Are there measurements of Rn concentration for dwellings above voids?
How many measurements of radon concentration in dwellings
Mean distance dwelling-void

1.4 Results

Among the 37 papers to evaluate, we found 3 main categories of papers: only **1** paper deals with the correlation of radon concentration measurements in voids and in dwellings above the voids, **29** papers deal with radon concentration in voids (mainly subway stations) and **7** papers deal with radon measurements in dwellings located in a karstic area.

The detailed description of the three main categories (as already described above) of papers is reported hereafter.

1.4.1 Correlation between voids and radon concentration in dwellings above voids

About correlation between voids and indoor radon concentration (IRC) in dwelling above voids, we found only one paper titled "Radon concentration in houses over a closed Hungarian uranium mine" [1].

In this paper, the concentration of radon in many dwellings above uranium mines has been measured. All dwellings are at various distances from the projection of the considered tunnel inside the mine. The radon concentration inside the mine tunnel is about 410 kBq/m^3 while the radon concentration in dwellings above the mine shows a clear step from 667 Bq/m^3 to 291 Bq/m^3 going from a belt within 150 m from the surface projection of the mine tunnel route to further 300 m distance. The tunnel is made of gray sandstone in which, the uranium content is relatively homogeneous over the tunnel and exceeds the crust world average by four to six times (U concentration is 11.5 ppm versus Word's value of 3 ppm).

Radon concentrations were measured in 129 homes for about 4 months, from December 2003 to March 2004, and the mean value measured for all dwellings is 483 Bq/m^3 compared to a national-wide average value of 134 Bq/m^3.

Since there is no significant difference between the gamma dose rate near the route of the tunnel and that measured at a greater distance, no different radon concentration, based on the radionuclide concentration, is therefore expected between the two areas.

Based on the scientific investigations undertaken, it was concluded that the radon existing in the mine tunnels influences the radon concentration on the surface. These measurements seem to suggest that, under certain circumstances, radon may emerge from an even greater distance (even as far as 50 m) and can influence the radon concentration on the surface.

1.4.2 Radon concentration in different types of voids

The papers reporting studies on radon concentration in voids of different types are 29. The main types of voids are subway stations but also caves and railway tunnels. In detail, there are 18 publications on subway stations, 8 on Caves, 2 on Railway Tunnels and 1 on Tunnel under Castle. (Table 8)

The radon concentration measurements in subway stations are usually very low (about a few tens of Bq/m^3 to 100 Bq/m^3), even considering that the tunnels have different geological compositions (granite, non-granite, tuff, limestone, etc.) and are at different depths in the underground. The low values depend mainly on the ventilation system inside the stations themselves. In fact, mechanical or natural ventilation in stations is always present (also simply for the passage of the train inside tunnels of the station, "piston effect"). The low values in these subway stations show also very weak dependence on the depth of tunnels and seasonal variations.

However, some stations are exceptions and show very high radon concentration values. In particular, we found 665 Bq/m^3 in Rome (Italy) [2] and 800 Bq/m^3 in San Paulo (Brazil) stations [3]. The Italian value could be influenced by the underground composition of volcanic tuff with a high radon concentration value, while for the Brazilian subway stations, the high concentration values could depend on the positions of monitors, situated away from the public circulation and also far from the train's routes.

Another important type of void analysed in this review is caves that, differently from subway stations, show very heterogeneous radon concentration values. The differences are linked to seasonal variations and the geological type of the caves themselves. In particular, a study in China [6] reports a detailed analysis of 55 caves of different geological types. In these caves the higher levels of radon concentration are for tuff and granite composition (200 - 300 Bq/m^3) versus andesitic porphyry with the lowest values about 50 Bq/m^3.

These values are, however, very variable in different countries. In fact, in Slovenia's karstic caves [4] we can find radon concentrations of thousands Bq/m^3 like in Italy (dolomitic limestones) [5] or in Romania (igneous and metamorphic rocks) [7].

In addition, there are also seasonal variations common to many caves. Generally, with some exceptions, the radon concentration in caves is higher in the summer period than in the winter period [4-7] even if with very different values. For example, in some of China's caves [6], summer-winter differences (for highest values) are very close (250 - 200 Bq/m^3). On the contrary, for caves in Slovenia [4] or in Italy

[5], the summer-winter values are respectively 6000 - 4000 Bq/m^3 and 1800 - 300 Bq/m^3. Also, for seasonal variations, we found an exception in Spain, in the Karstic caves of Altamira [8], where radon concentrations in the summer period are lower than in the winter period and are respectively in the ranges (300 - 700) Bq/m^3 and (3200 - 5700) Bq/m^3.

Two papers [10, 9] deal also with railway tunnels in Fujian (China) and in Alicante (Spain). In Fujian, the main geology is granite with a radon concentration value of 1160 Bq/m^3. In the study of Alicante, the measurements, in two different tunnels, are compared. The first tunnel (ventilated) had a radon concentration value of 45 Bq/m^3 and the second tunnel (not ventilated) had a radon concentration value of 900 Bq/m^3.

Table 8 - Values of radon concentration in different City and for different types of voids and different geology. In square brackets bibliography reference.

Country(years)	Radon Concentration (Bq/m^3)	Geology Type	Void's Type (#)
China	**(Summer-Winter):** (250-200) Granite, (300-130) Tuff, (40-70) Andesitic porphyr, (200-180) Quartz Sandstone, (140-50) Limestone.	Granite, Tuff, Andesitic Porphyr, Quartz Sandstone, Limestone	**Caves (55)**: Granite (28), Tuff (5), Andesitic Porphyry (7), Quartz Sandstone (5), Limestone (10)
China. Guiyang	<25	Porphyry	Subway stations
Spain. Alicante (2015-2016)	First Tunnel 45 (ventilated). Second Tunnel 900 (not ventilated)	Limestone rocks	Railway Tunnels (2)
Slovenia (1998-2001)	Range (1500-4000) in Winter. Range (4000-6000) in Summer	Karst Caves	Karst Caves
Tokyo (August-November 1994)	11, range (7-24)		Subway stations (7)
China. Beijing (2017-2018)	12 in operation and 120 during construction	Clay silt	Subway stations (1)
Seoul (1989-1991)	range (150-300) for almost stations	Granite bad rock	Subway stations (74)
Poland	range (1000-8000) with different seasonal variations	Metamorphic rock caves	Caves (2)

Country(years)	Radon Concentration (Bq/m^3)	Geology Type	Void's Type (#)
Italy. Savona (2000-2001)	range (1000-1800) may-nov. range (50-300) nov-may.	Karst zone in dolomitic limestones	Caves
Honk Kong	42, range (30-60). Higher than dwellings (30)	Granite	Subway stations (31)
China. Shaanxi (2004-2005)	range (400-2000)	Karst Cave	Caves
India. Kolkata	23, range(14-48)	Crust of low radon level	Subway stations
Italy. Roma	665	Vulcanic Tuff	Subway stations (1)
Brasil. Sao Paulo	800 (subway), 4800(gold mine)		Subway stations (15), Caves of gold mine (14)
Venezuela	range (100 - 80000)	Caves Karstic	Caves
Korea. Seoul	range (19-114)	Granite bad rock	Subway stations
Korea. Seoul	28, range (9-86)	Granite bad rock	Subway stations (267)
Spain. Altamira	range (300-700) Summer. Range (3200-5700) Winter	Caves Karstic	Caves
China. Fujian	1160 (railway), 359 (Shelters)	Mainly Granite	Railway Tunnels, Shelters
Czechia. Prague (1995)	range (11-15)	Rocks, limestone	Subway stations (20)
Korea. Daejeon (2007-2008)	34	Granite bad rock	Subway stations (22)
Korea. Seoul (2013 and 2015)	26	Granite and non-granite rocks	Subway stations (100)
Korea. Seoul (2013 and 2015)	37	Granite bad rock	Subway stations (40), Parking Lots (19)

Country(years)	Radon Concentration (Bq/m^3)	Geology Type	Void's Type (#)
Poland (2017-2018)	1000	Sedimentary, mainly including clays, siltstones and sandstones	Tunnels
Iran. Teran (2005)	14	Bedrock (calcite) and sedimentary stones	Subway stations (16)
Finland. Helsinki	100	Bedrock	Subway stations (4)
Romania	Cold Season range (300-800), Hot season range (400-2400)	Igneous and metamorphic rocks	Caves (7)
Venezuela. Caracas	30	Igneous and metamorphic rocks	Subway stations (35)
Uzbekistan. Tashkent	<40 except 3 station range (50-170)	Bedrock (green tuff), carbonate, siliciclastic	Subway stations (23)

1.4.3 Mean radon concentration in dwellings above karstic zones.

In different regions of Europe, measurements of IRC in dwellings above karstic zones show levels above the average of the region itself.

The seven papers found on this topic deal with single dwelling measurements, a large number of schools, or extensive measurements in the whole country. The papers cover years from 90's to 2019. Besides, also very different measurement periods are used (ranging from weeks to months) even in different seasons.

Despite all differences, the karstic zones, even if they have a low level of uranium content, can show a high level of IRC due to cracks or fissures in soil that can allow radon to move for many meters. For these reasons, value of radon concentration in dwellings above the karstic zones can range from a few tens to thousands of Bq/m^3.

All interesting information collected from papers is reported in Table 9.

Table 9 - Radon Concentration values in dwellings over karstic area for different countries. In square brackets bibliography reference.

Country (years)	Geology	Measurement period	Places monitored	Radon Concentration (Bq/m^3)
Italy. Lecce (2018-2019)	Karst Area	12 months	963 rooms in 54 buildings	161
Ireland. Castleisland (1992-2017)	Different types of geology	3-12 months (seasonal adjusted)	180 points	10 to 49000. Clare Shales and Dirtoge limestones values 100-1000. Other types 10-100.
Switzerland (1987-1991)	Karst Area	2-3 months	dwellings	10 to 10000
Slovenia (2011-2012)	Sedimentary rocks of Karst Area		Single dwelling (2 rooms)	1200 (ground floor) and 7000 (first floor)
Lithuania (1995-1998)	Karst Area	Summer	400 dwellings	55. 125 in karst region
Ireland (2004-2012)	Karst limestone area	Winter	Single dwelling	1500 to 450 (after remediation)
Slovenia (1992-1994)	Karst Area	Winter	890 schools	168. (range 73 - 318 due to geology).

In particular, we found that in karstic zones, IRC has higher values than in non-karstic zones. For example in Lecce [11] the investigated zones (karstic) show values of IRC higher than in the whole Puglia Region.

In Ireland [12] we found different values of IRC correlated with different types of geology. In particular an IRC variability from a few Bq/m^3 to 49000 Bq/m^3 has been found in 180 measurements. Part of the variability is linked to bedrock geology and soil-gas content.

In Switzerland [13], where there are extensive karstic zones, the IRC is around 60-70 Bq/m^3 but in the mountainous zones the IRC is even 10000 Bq/m^3.

A publication with measurements in 400 dwellings in Lithuania [14] shows that the mean value of radon concentration is about 55 Bq/m^3 but in the karstic zones, this value grows up to 125 Bq/m^3.

In Slovenia, 890 schools [15] were measured in the winter period and the results show an IRC of 168 Bq/m^3 with higher values (up to 318 Bq/m^3) in the karstic region.

2 Performed Analysis

Introduction

To study the influence of local underground voids on radon levels in dwellings located above voids, the first step has been to collect datasets considered suitable for this purpose. In particular, the main work has been focused on gathering information both on voids (type, position, depth, etc.) and on dwellings (position, mean radon concentration, floor, etc.) from each partner.

Each partner worked with their own datasets in order to describe them in detail, both for voids and for dwellings. Each partner has conducted analysis to investigate any potential correlation between the presence of voids and indoor/in soil radon concentration.

Beside the analyses of correlation between voids and radon concentration in dwellings (above voids) are interesting also to characterise different types of voids.

The analysis of the correlation between the presence of underground voids and radon concentration values represents a fundamental area of investigation in the context of radiation protection and the understanding of geogenic factors that influence radon exposure. The general objective of these analyses is to determine if and how the proximity or presence of such underground structures can influence the levels of radon present in the soil and, above all, in indoor environments.

2.1 Austrian analysis

2.1.1 Introduction

IRC depend on multiple conditions as the geogenic radon potential (e.g. permeability, uranium content of the soil), the technical standard of the building (e.g. sealing against the underground) and the usage of the building (e.g. air ventilation rate). Radon hazard mapping assigns the geogenic radon potential to areas and locations, which should best reflect the environmental contribution to IRC. In this study we analyse the possible effects of karstificable lithologies, geological faults and artificial underground voids on IRC. Therefore, we use an exhaustive IRC data set from Austria, geological maps and a dataset of mining sites in Austria.

Austria features a high diversity of geological units due to the Alps, its surrounding basins, the younger deposits of the last ice ages and the much older basement of the variscan orogenesis (Bohemian Massif). Especially in the Alps some of these lithologies, mostly carbonates and their low-grade metamorphic alterations, are karstificable. Karstic landforms feature a high underground permeability, which could have a potential impact on the geogenic radon potential. Figure 1 shows the distribution of IRC for different lithologies. Typically, in all lithologies high IRC can be found, which resembles that the IRC depends on multiple factors. The crystalline rocks of the Bohemian Massif show the highest median IRCs and is generally one of the regions in Austria with the highest geogenic radon potential. Also carbonates show high median IRC, which can be linked to the composition of the rocks but also potentially due to karstic features, which increase the permeability of the underground

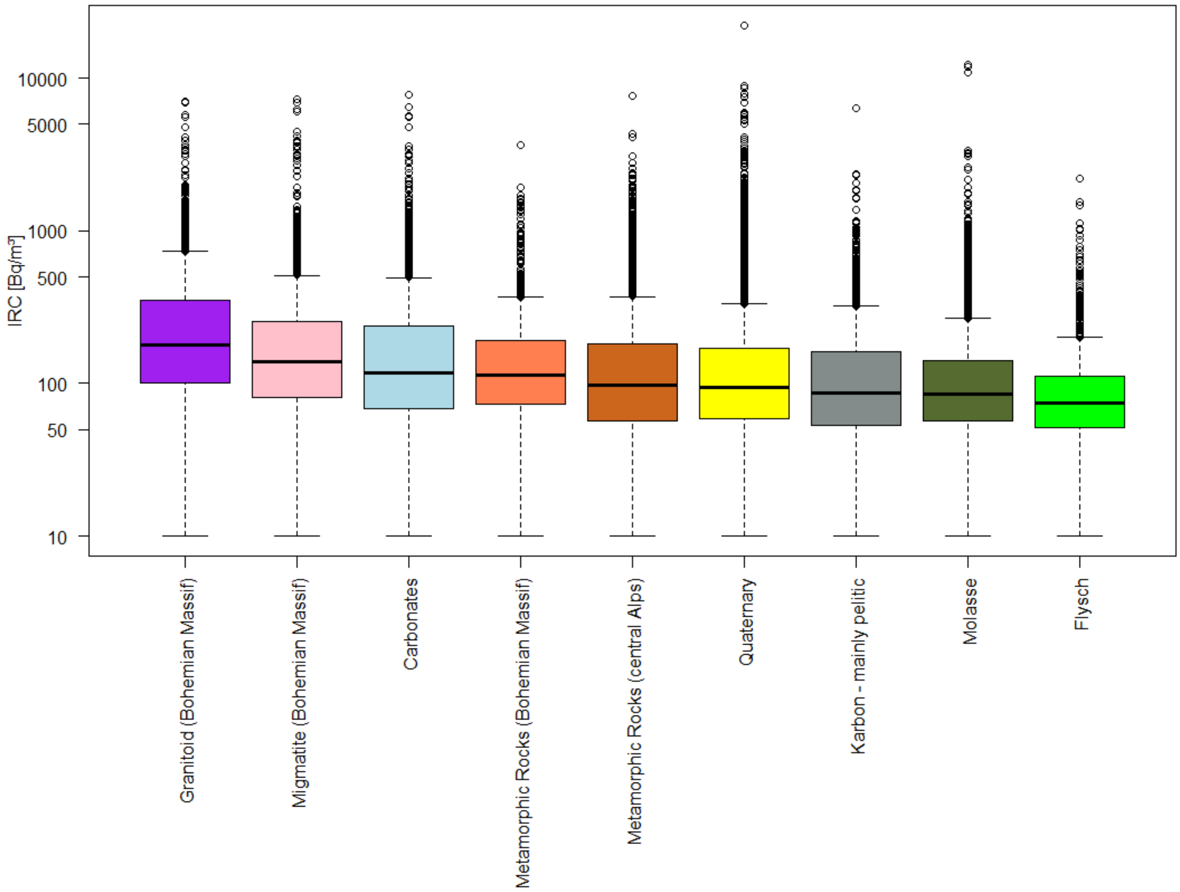

Figure 1 - Distributions of IRC within different lithologies in Austria. The lithologies are ordered by median and the y-axis is in logarithmic scale. Only lithologies where at least 1000 measurements are present are shown.

Geological faults can also have an impact on the geogenic radon potential, by altering the pathways for radon in the underground. Also, artificial voids in the underground can have a possible effect on the geogenic radon potential. We do a descriptive statistic and especially analyse if the distance to features as faults or mining sites has an impact on the geogenic radon potential.

2.1.2 Data and methods

The source for the IRC is an exhaustive radon survey in dwellings measured nationwide in Austria [38]. Over 25,000 occupied dwellings have been measured with track etch detectors. The measurement time was six months, half in the winter and half of it in the summer, and two detectors were supplied to every household. Along with the IRC for each sample additional variables as building characteristics and environmental conditions are included in the data set. The sampling design was spatial representative, where in each community a similar number of measurements was intended. Therefore, the Austrian indoor radon data set can serve as a profound basis to analyse the impact of environmental features on IRC. In this study we are interested in the geogenic radon potential and want to minimize the contribution of other factors as building characteristics. Therefore, we only use a subset of IRC measurements for our analysis and filter the data set to IRC measured on the ground floor and basement.

The Austrian Geological map [39] in a resolution of 1:500,000 is the source for lithologies and faults. About 2000 of the measured dwellings are located on lithologies that are capable of karstification. Figure 2 shows the positions of those dwellings in Austria, color-coded for different levels of IRC. The karstificable lithologies are spatially inhomogeneous distributed, where most of them are in the northern calcareous Alps (Figure 2, turquoise broad band in the middle of Austria). Also, spatial clusters of high and low IRC can occur.

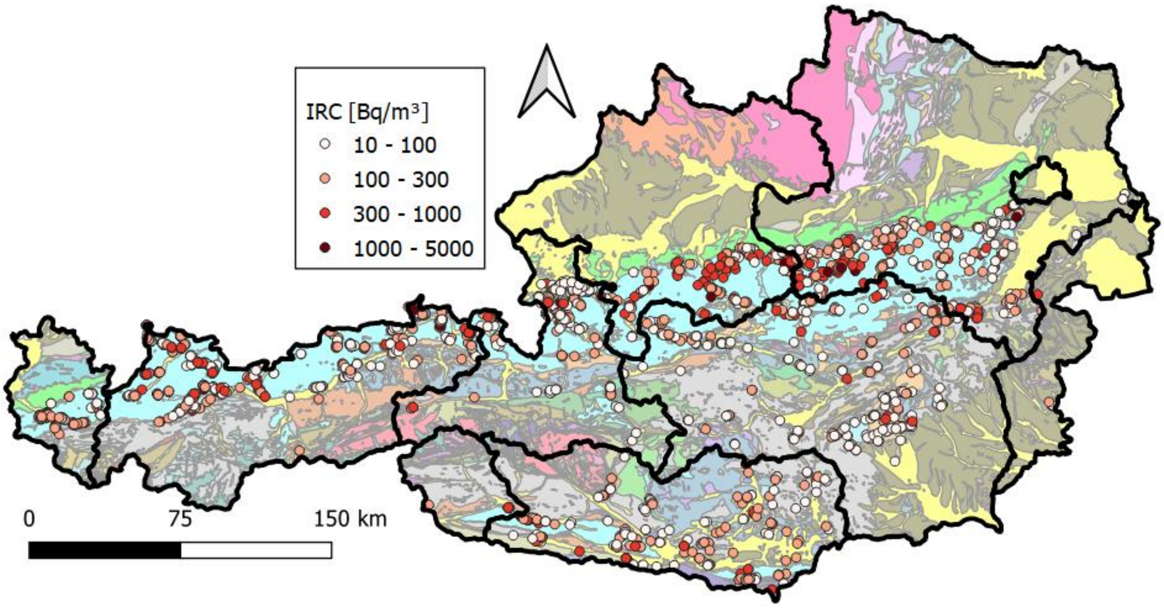

Figure 2 - Map of Austria highlighting the IRC of dwellings in lithologies that potentially developed karstic landscapes. The IRC are color-coded for different levels. In the background the geological map of Austria is shown, highlighting karstificable lithologies.

In addition, a dataset of mineral resources in Austria was analysed [40]. The data features occurrences, prospections and mineral deposits in Austria including parameters as the type of commodity and dimension of the site and the position of the centre of the site. We are interested in anthropogenic underground voids associated with mining activities and therefore filtered the data set to mining sites in which underground voids are certainly present. Doing so, 206 mining sites could be acquired for our analysis.

We analyse IRC distributions for different lithologies, especially focusing on the distance to geological faults and mining sites. Therefore, we use descriptive statistics, correlation analysis and visual analytics.

2.1.3 Results

In the Introduction (Figure 1) we already showed that the carbonates associated with karstic landscape feature one of the highest median IRC, where only the crystalline rocks of the Bohemian massif show higher median IRC in Austria. Figure 3 shows distributions of IRC for different karstificable lithologies. The different lithologies show different median radon levels, but also within one lithology, a high variability of radon concentrations is possible. This variability might be associated with geogenic conditions as composition or the permeability of the rocks. Overall, the most IRC data are located in the northern calcareous alps (carbonates Trias-Jura) which also show one of the highest median IRC.

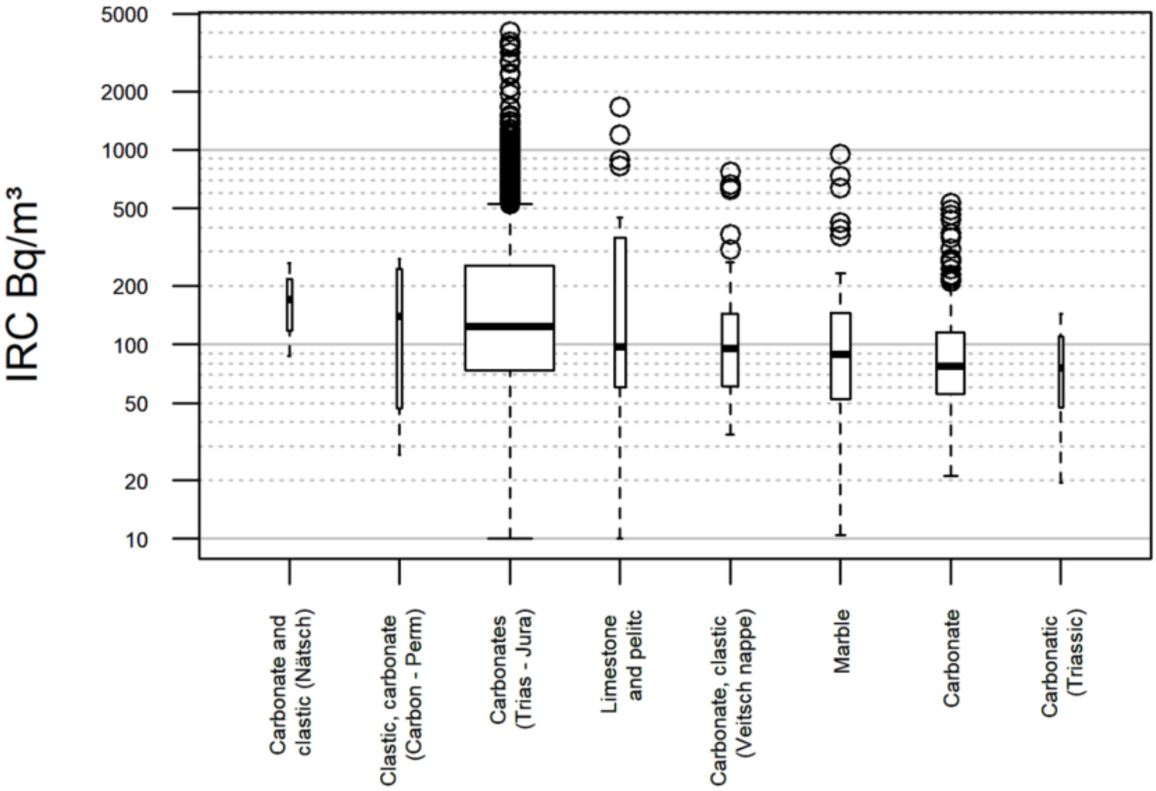

Figure 3 - Distribution of Radon concentrations for different karstificable lithologies in Austria shown as boxplots. Y-axis is logarithmic. The width of the boxes is relative to the number of observations

The distance from faults might have an impact on IRC, due to altering the pathways for radon. Therefore, we further analysed if the distance from faults influences the IRC. We separated this analysis in lithologies which can feature karstic landscapes and all other lithologies. Figure 4 shows the IRC distributions of these two lithological groups and for different distances from geological faults. For both lithological groups the differences in IRC distributions due to distances from geological faults are only minor, where the highest median IRC can be observed for distances of 10-50 meters and greater than 5 km from geological faults. The median IRC are alternating between high and low values, and no clear trend can be observed. For all distance classes the karstificable lithologies show higher IRC median values compared to the non-karstificable lithologies and again in all distributions high and very high IRC are present.

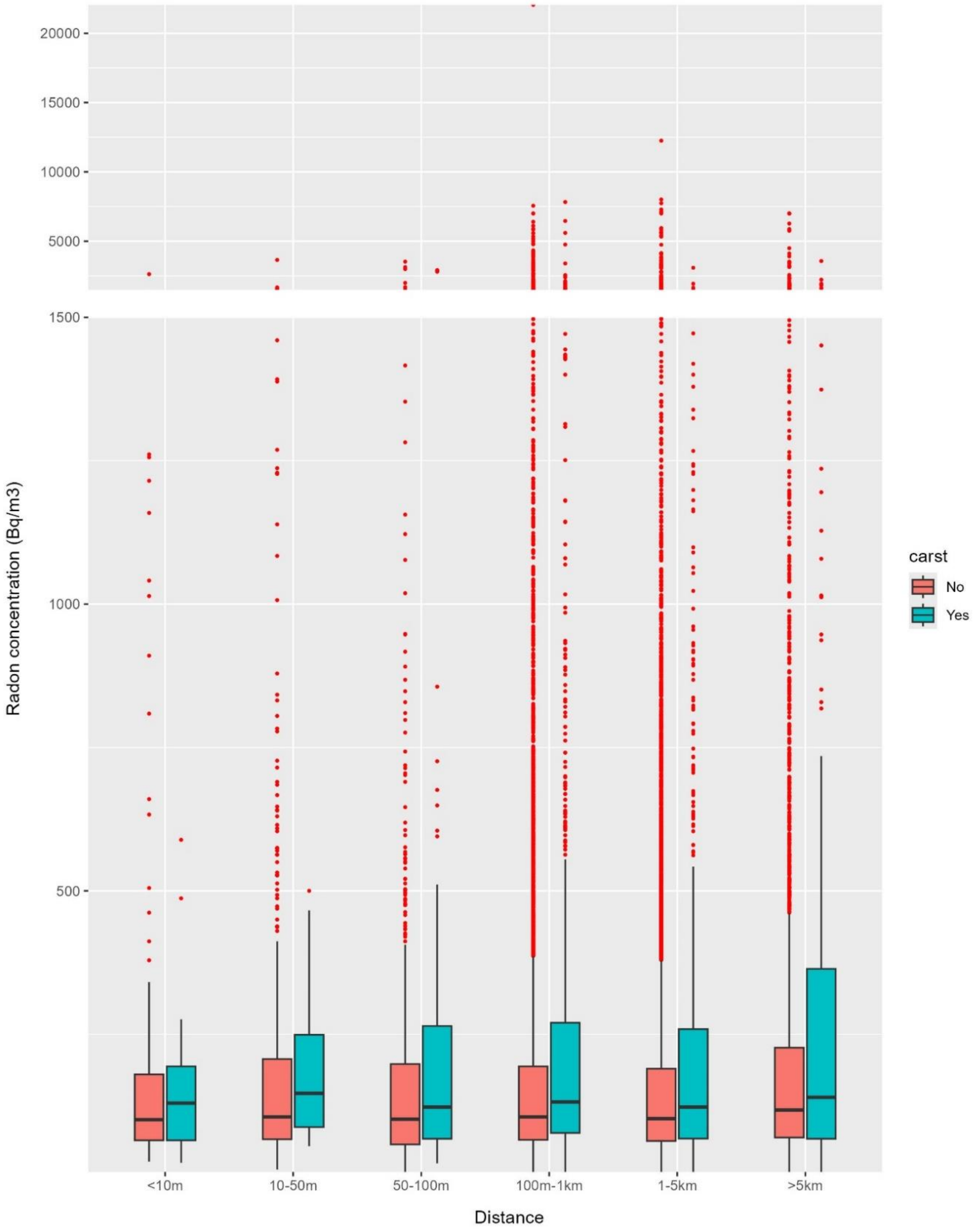

Figure 4 - IRC distribution for karstificable lithologies and all other lithologies grouped for different distances to geological faults.

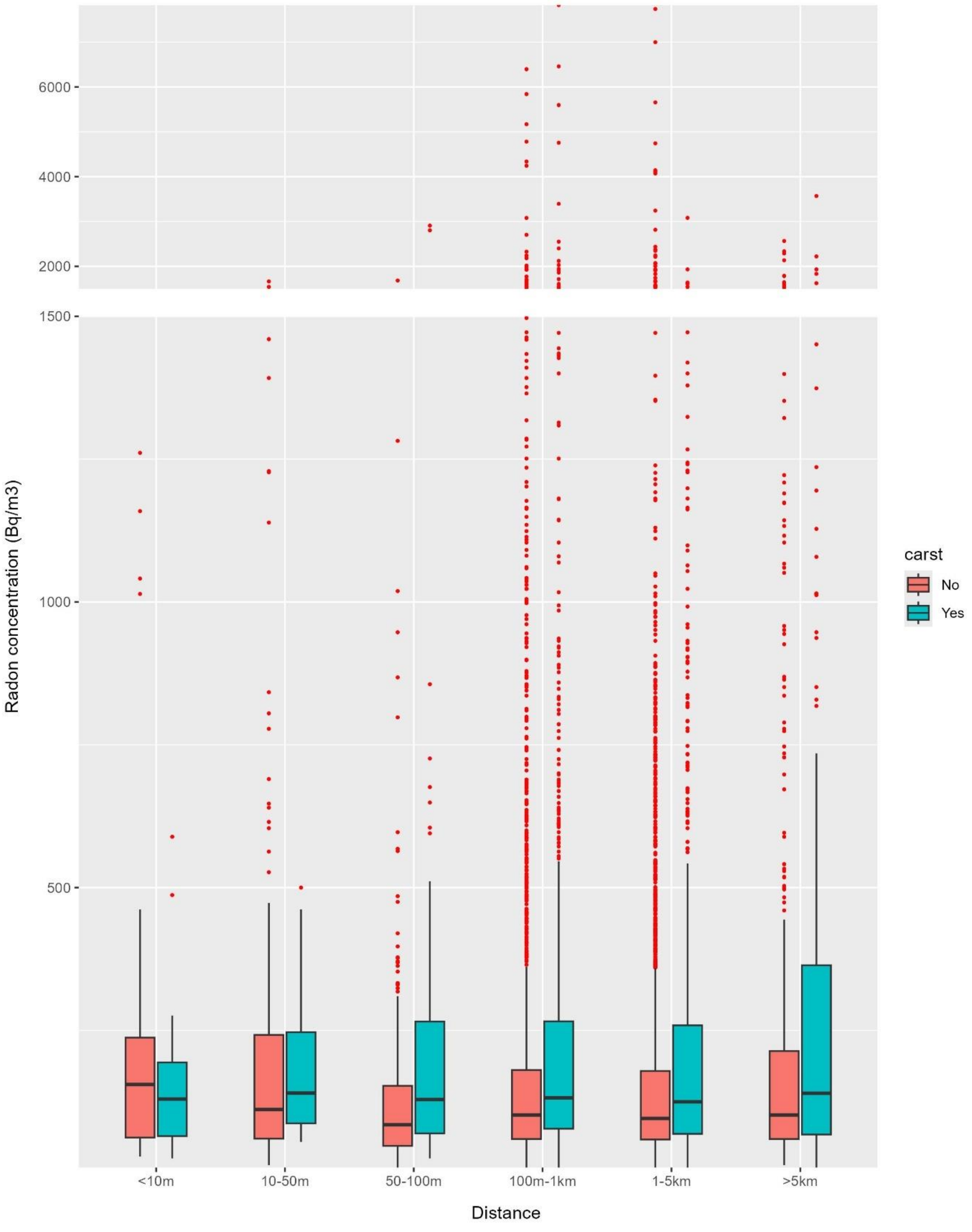

Figure 5 - IRC distribution for alpine karstificable lithologies and other alpine lithologies depending for different distances from geological faults.

The dataset for geological faults features different fault densities for different lithologies. For the crystalline rocks of the Bohemian massif only very few faults are present. Alpine lithologies feature much more geologic faults. Also, the lithologies of the crystalline rocks of the Bohemian massif show the highest median IRC. This might influence the relationship between IRC and the distance from geologic faults. Therefore, we repeated this analysis but only using lithologies of the main body of the alps in Austria: austro-alpine, penninic and helvetic nappes. Figure 5 shows the results of this analysis. For the non-karstificable alpine lithologies decreasing median IRC can be observed for distances smaller than 100 m to the faults. For distances > 100 m the median IRC and distributions are comparable. The karstificable lithologies were already discussed in the previous analysis.

We shifted our analysis from karstic environments and geological faults to anthropogenic underground voids associated with mining sites. Overall, we analysed 206 sites which show underground voids. The sites feature various mineral deposits and different depths of the mining site. Figure 6 shows IRC distributions for different distances from these mining sites, separated for shallow (<= 100 m) and deep (>100m) mining sites. The distributions closest to the mining sites (0 – 100 m) show the lowest median IRC for both subgroups. But one needs to keep in mind, that the number of IRC measurements close to the mining sites is very small compared with measurements taken further away. The shallow mining sites show the highest median IRC in a distance range from 100 to 500 m and a decreasing trend with increasing distances. The deep mining sites show the highest median IRC from 0.5 to 1 km, and from there on also a decreasing trend for IRC with increasing distance.

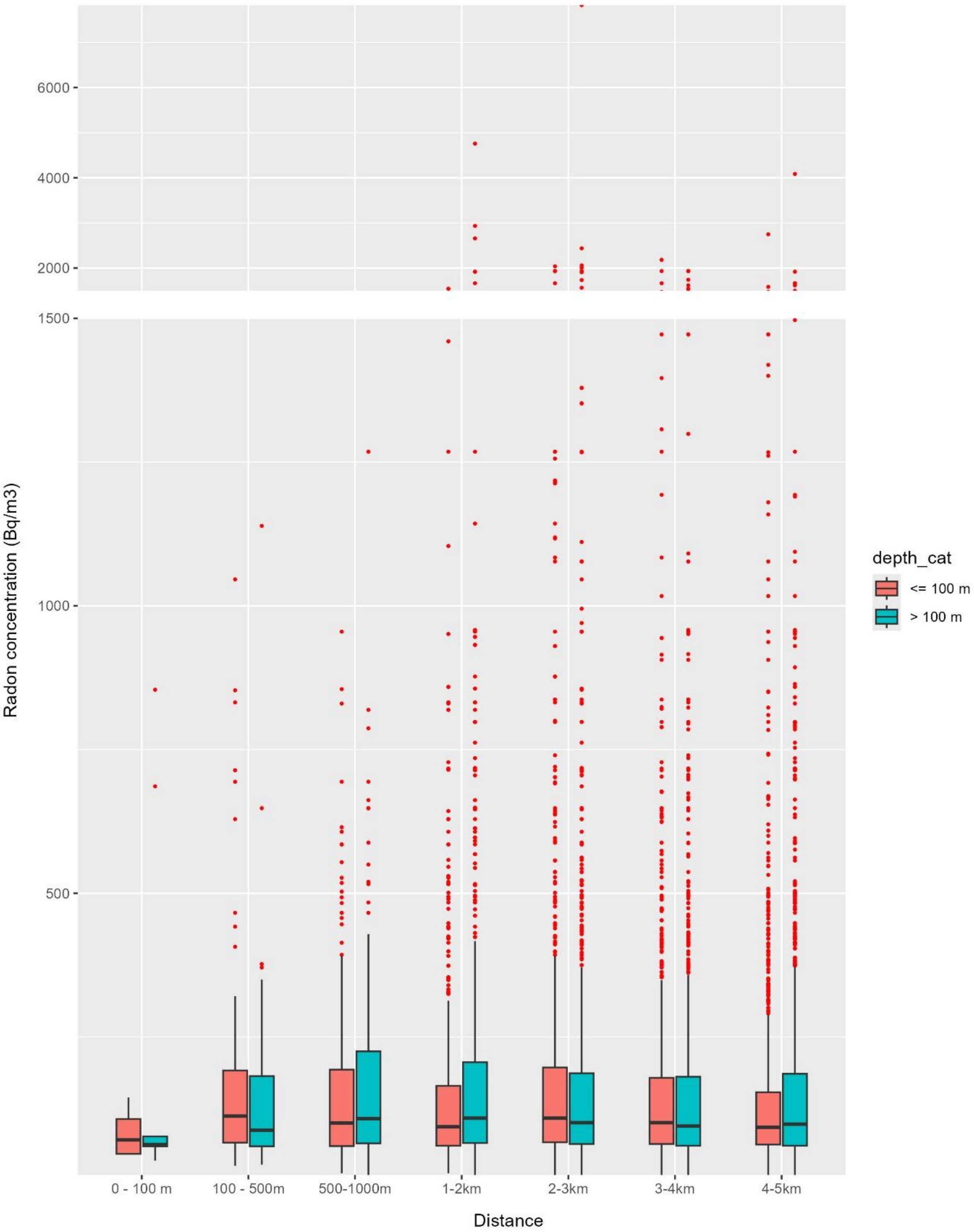

Figure 6 - IRC distributions for different distances from mining sites with underground voids for shallow and deep mining cites.

The previous analysis shows that an effect of anthropogenic underground voids for mining sites on IRC distributions is possible. We refined our analysis by doing a correlation analysis of IRC and distance to the mining sites for single sites. We only used sites where at least 50 IRC measurements are present within a radius of 5 km to obtain robust results. Doing so, 85 sites were analysed. We use the Spearman correlation factor to be able to detect non-linear relationships as well. Out of the 85 sites 11 sites showed correlation factors greater than 0.3 or less than -0.3 between IRC and distance from the site (Table 10). Eight sites show positive correlations, featuring both shallow and deep mining sites. The main commodity of the sites with positive correlation is brown coal, but also metal deposits are present. Three sites show negative correlations between IRC and distance from the sites. Here only deep mining sites are present, and interestingly also one brown coal commodity. Figure 7 gives a visual impression of the mining site with the highest and lowest correlation factor.

Table 10 - Mining sites with underground voids with at least 50 IRC measurements in a radius of 5 kilometres from the site and a correlation between IRC and distance from the site higher than 0.3 or lower than 0.3.

Commodity	rho (IRC ~ distance)	Depth [m]	mean IRC	n IRC
copper, antimony, nickel, silver	-0.45	360	121	54
pyrite, copper	-0.44	120	286	54
brown coal	-0.32	330	168	60
brown coal	0.33	52	107	66
brown coal	0.35	130	76	56
copper, antimony, lead, zinc, silver	0.35	330	138	99
brown coal	0.36	20	82	51
brown coal	0.37	240	104	91
pyrite, copper, lead, zinc	0.39	230	268	67
copper, silver, antimony	0.42	120	147	103
brown coal	0.45	42	117	66

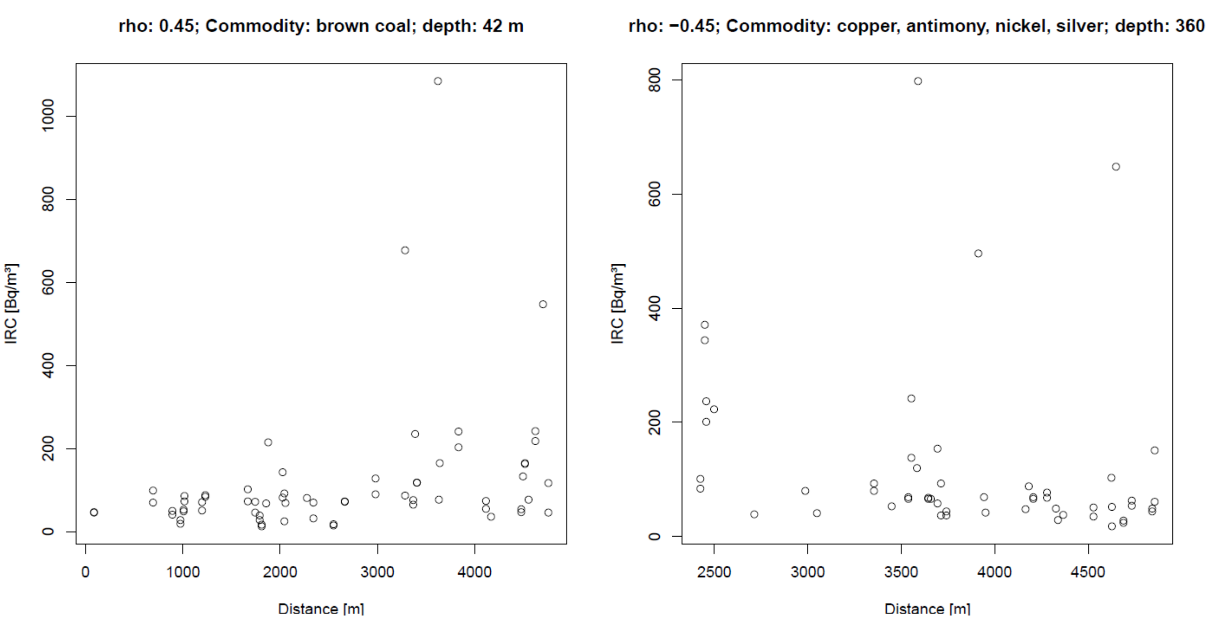

Figure 7 - Scatterplot of the two mining sites showing the highest correlations among sites with underground voids and more than 50 IRC measurements in a radius of 5 km to the site

2.1.4 Discussion

Different environmental conditions can influence the IRC and the geogenic radon potential. In this study we analysed if karstificable lithologies, the distance from faults and the distance from mining sites with underground voids have an effect on IRC. We found that in Austria karstificable lithologies show one of the highest IRC distributions, where only the crystalline rocks of the Bohemian massif show higher IRC distributions. Within these karstic lithologies different levels can also be found, and spatial clusters can be observed. For all lithologies in Austria the distance from geological faults does not affect the IRC distribution, which is especially true for the karstic lithologies showing alternating higher and lower IRC distributions with increasing distance from geological faults. For the subset of the alpine lithologies a weak decreasing trend of IRC levels with increasing distance from geological faults can be observed.

The effect of distances from mining sites on IRC does also not show a clear trend. Both, negative and positive correlations could be found for single sites. Overall – except for IRC measurements very close to the mining site (<100 m) – a decreasing trend of IRC with increasing distance could be found on shallow and deep mining sites. Underground voids can have multiple effects on IRC of dwellings on the surface. Increasing the permeability of the underground could potentially increase the pathway for radon in the underground. On the other hand, underground voids close to surface could also be seen as a radon “reservoir” possible decreasing the exhalation rate of radon at the surface. Also, other possible effects of mining sites on IRC must be considered. The excavation material of mining sites could be used as filling or “artificial” underground, where later dwellings are built. This could change the composition of the underground and the grain size of the soil, which has potential effects on the IRC.

Our analysis shows karstic lithologies show one of the highest IRC distributions. Clear overall trends regarding the effect of distance from geological faults and distance from underground voids associated with mining sites could not be detected. But for single mining sites both negative and positive correlations were found. Also, for a subset of lithologies (alpine nappes) weak trends between distances from geological faults and IRC was found.

2.2 Czech Analysis

2.2.1 Introduction

In the Czech Republic, IRC have been measured since 1990, these measurements continue up-to-day according to the interest of home owners and remains for all Czech residents for free. Thus, Czech national radon database contains more than 170,000 results obtained in schools in use, occupied family houses and flats.

2.2.2 Data Description

All the measured data have been obtained by track-etched detectors with one-year measurement exposition from 2002. Shorter measurements (exposition time: 2 months in the heating season) were also included. For one flat, two detectors were handed out. Along with IRC, identification and characteristics of dwellings and examined rooms have been also recorded, e.g. material of walls, tightness of windows, or subjective evaluation of ventilation rate.

The other sources for this analysis are two geological maps prepared by the Czech Geological Survey: namely the prognostic map of radon index of the area (shown in the Figure 8), and the map of undermined areas (see Figure 9). These maps are available online on the server of the Czech Geological Survey and can be used for various analysis. Areas with low radon index are marked with light yellow, medium index areas are ochre and high index areas are red.

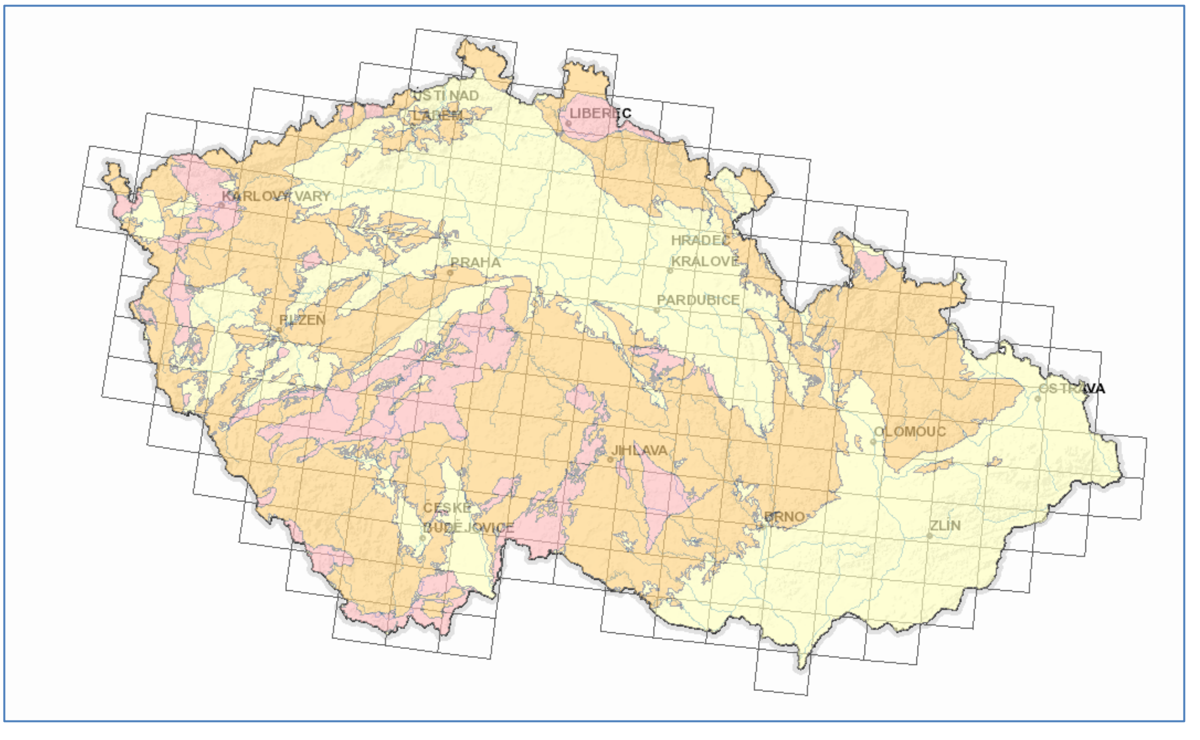

Figure 8 - Prognostic geological map of radon index (Czech Republic), Czech Geological Survey

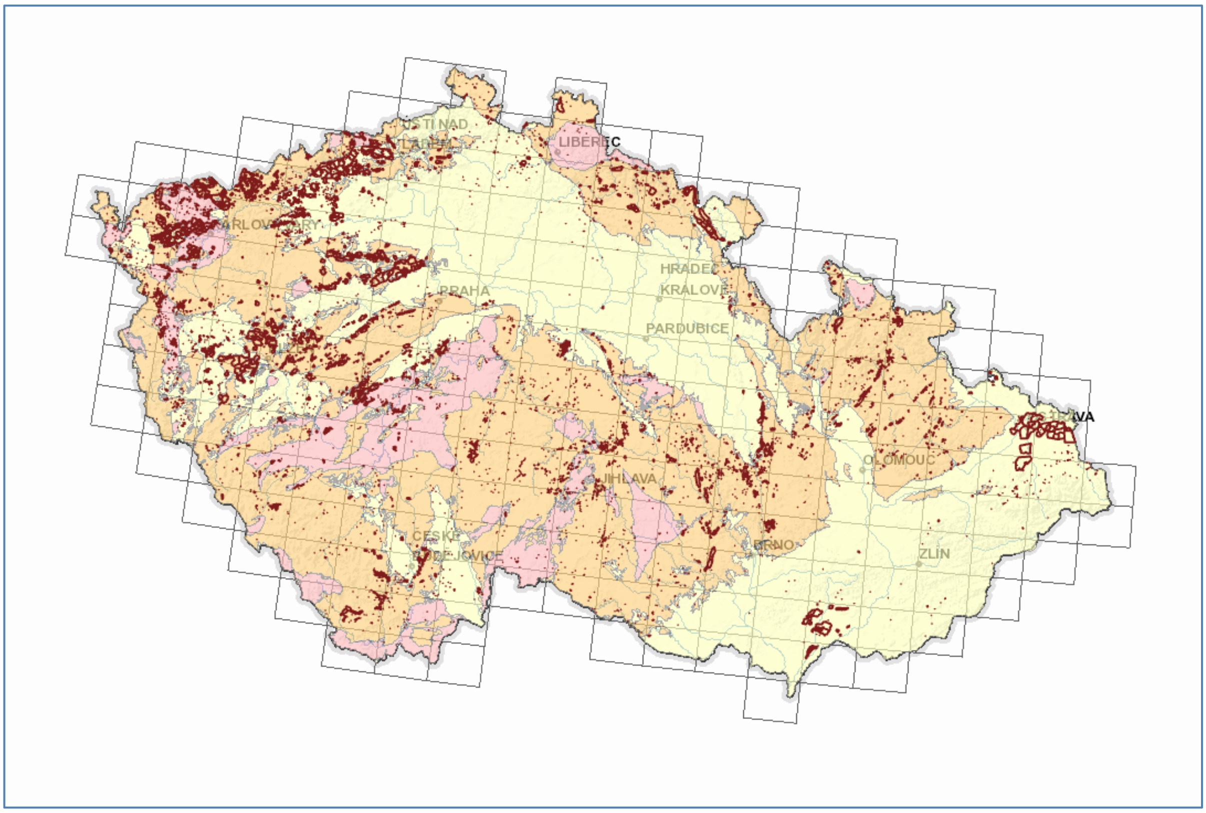

Figure 9 - Geological map with undermined areas, Czech Geological Survey

For the analysis, the north-west part of Bohemian building stock has been chosen, namely built on areas characterized with low radon index situated in localities with mining industry. In these areas with coal, kaolin, swag or precious metals mining, a lot of underground voids, shafts or misused and closed mines can be found. The detail of these areas is shown in the Figure 10.

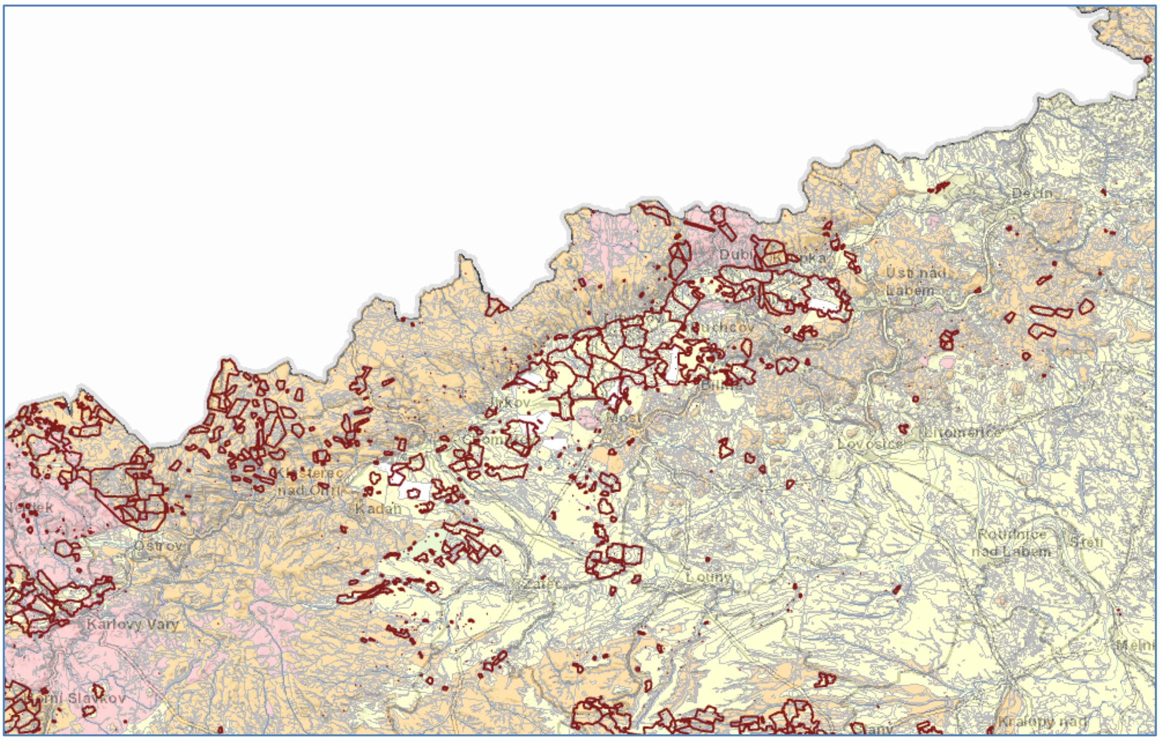

Figure 10 - Detail of the geological map with undermined areas, light areas taken into analysis

The distances of undermined areas from the measured houses were generated by merging the positions of undermined areas and dwellings using tools available on the server (see Figure 11).

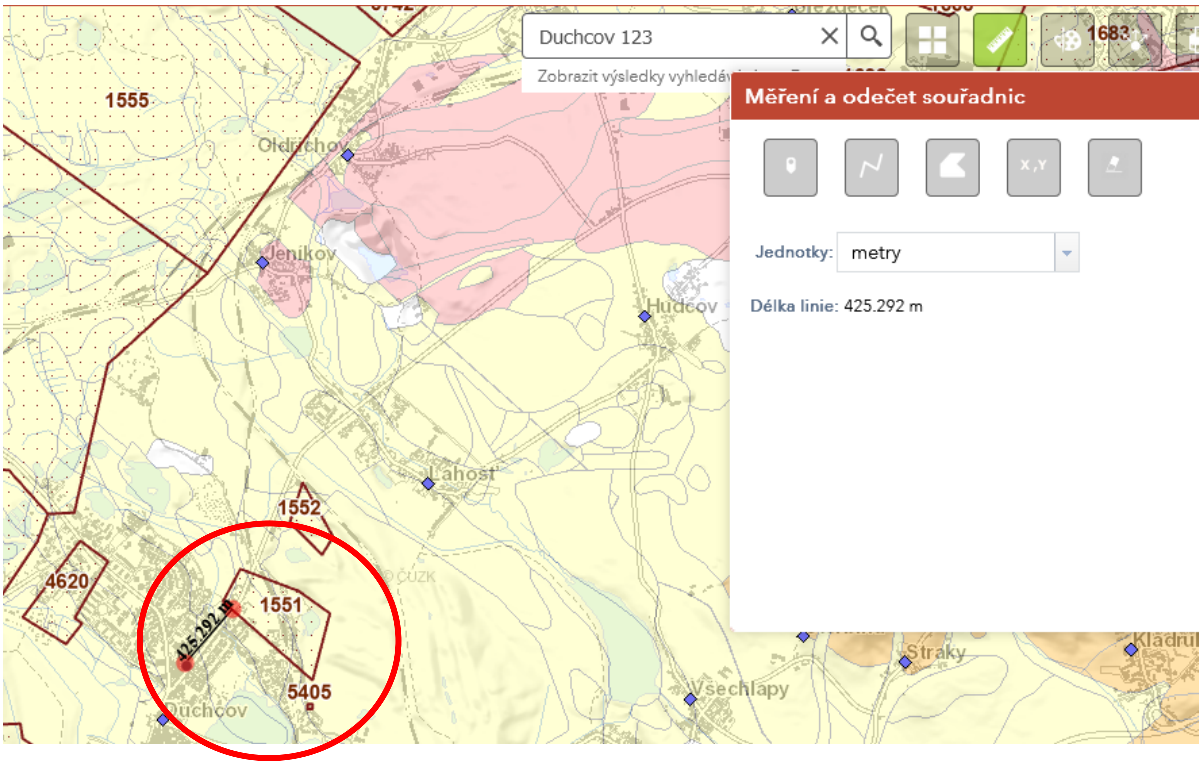

Figure 11 - Detail of the geological map with the tool for distance measurement

Only results from family houses with known addresses were used for the analysis. In this way, two smaller datasets have been prepared, later used for calculations. The datasets description is reported in Table 11 and Table 12.

Unfortunately, the distance has been determined only by the tool given in the map, which was not precise enough. The use of GPS for objects (buildings and undermined polygons) should certainly give more accurate results. Nevertheless, the accuracy is sufficient for the purpose of this pilot study.

Table 11 – Description of the dataset of radon concentration measurements in buildings on not undermined areas

Dataset Variables	Description of variable
ID_Dwelling	Unique identifier for dwelling
Region	Identification (code) of the region
City	Identification (code) of the municipality
Building address	Street and number of the dwelling
Annual mean radon concentration (Bq/m^3)	Value of mean radon concentration in dwelling in Bq/m^3
Annual maximum radon concentration (Bq/m^3)	Value of maximum radon concentration in dwelling in Bq/m^3

Table 12 – Description of the dataset of radon concentration measurements in buildings in municipalities being fully or partially undermined

Dataset Variables	Description of variable
ID_Dwelling	Unique identifier for dwelling
Region	Identification (code) of the region
City	Identification (code) of the municipality
Building address	Street and number of the dwelling
Annual mean radon concentration (Bq/m^3)	Value of mean radon concentration in dwelling in Bq/m^3
Annual maximum radon concentration (Bq/m^3)	Value of maximum radon concentration in dwelling in Bq/m^3
Distance from undermined area in the municipality (m)	The distance of the building from the undermined area in the municipality in meters (0 for buildings located above undermined area)

2.2.3 Results

The first analysis performed on the two datasets (radon concentration measurements in undermined and not undermined buildings) aims to evaluate potential difference between the radon concentrations in dwellings above voids from those in houses on solid ground.

From the first dataset, 182 measurements in buildings on the solid ground were taken into analysis. The distribution of mean radon activity concentration (RAC) value is shown in the Figure 12.

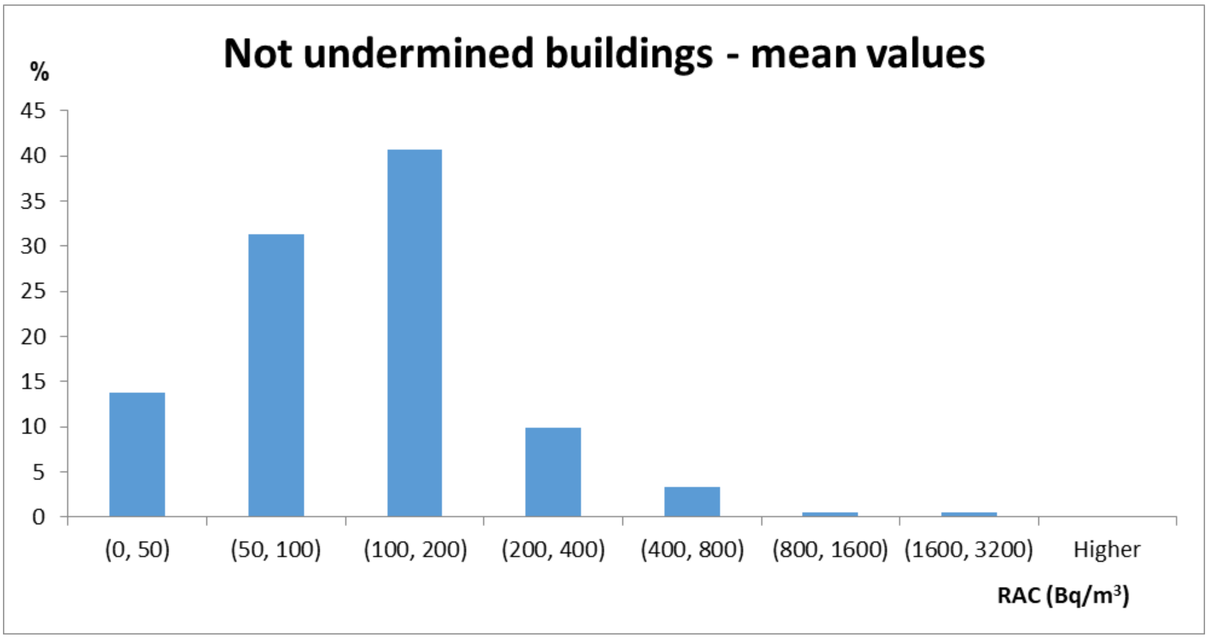

Figure 12 - The distribution of mean radon concentrations in buildings on solid ground.

The concentrations in buildings from municipalities not being undermined are compared to those obtained from 64 buildings standing on undermined polygons in the municipalities with undermined territories. The distributions for mean value in buildings are depicted in the Figure 13. The statistical characteristics are shown in the Table 13.

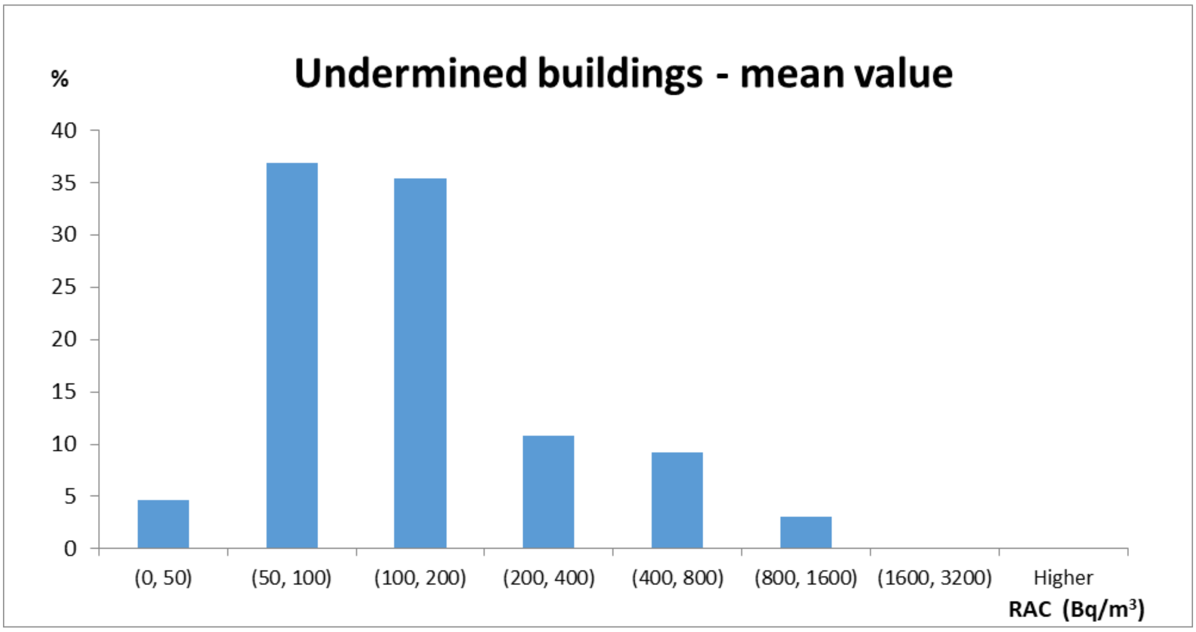

Figure 13 - The distribution of mean radon concentrations in buildings on undermined polygons.

Table 13 - Statistical characteristics of both groups of objects

Group	Mean RAC (Bq/m^3)	SE	Number
Buildings on solid ground	**144**	**163**	**182**
Undermined buildings	**199**	**204**	**64**

Unpaired statistical T-test has been used to evaluate the difference between both groups. It confirmed that the groups of buildings differ from each other on the statistical level α=5 %, where the higher values belong to undermined buildings.

The second analysis performed on prepared dataset (formed in municipalities on partly undermined areas, database structure see Table 11) was trying to find a correlation between the IRC and building distance from the undermined polygons, in intervals given by 100 m (0,100), (100,200), until 500 m. The results are shown in the Table 14.

Table 14 - Mean radon concentration versus distance of the building from the undermined polygon

Distance from the undermined polygon (m)	Mean RAC (Bq/m^3)	SE	Number
0	199	204	64
(0, 100)	162	127	27
(100, 200)	158	155	38
(200, 300)	101	65	22
(300, 400)	108	38	7
(400, 500)	152	164	12

It can be seen that the highest concentration can be found directly above the undermined polygons, the houses located in different distances from the polygon edge are lower, no relation of radon concentration with elevated distance of the buildings until 500 metres has been found.

Unfortunately, the number of houses analysed is too low to reveal some effects, more populated samples (maybe joint samples from more districts) are necessary.

2.3 French Analysis

2.3.1 Introduction and site description

High levels of radon-222 inside buildings have been monitored over the years in the French Jura Mountains, close to the Swiss borders. The geology of this area consists mainly of Jurassic limestone rocks with numerous karstic displays. Limestone contains small amounts of uranium-238 and radium-226 and is therefore generally not considered to be a significant source of radon release [41]. However, strong enrichments of radium-226 compared to the activities of uranium-238 have been observed in limestone karst soils of the Jura Mountains [42]. Such radium enrichments in soils may explain the high levels of radon observed in the indoor air of buildings. Furthermore, karst environments are highly fractured and permeable media with numerous voids. It is therefore also possible that the high radon levels observed in buildings are linked to radon transfers from deeper layers or from karst voids.

In order to quantify the impact of radium-226 activity in soils and the influence of karst voids, a study was carried out on a pilot area in the Jura Mountains including the acquisition of field data and the development of a numerical model which can simulate radon transport in karstic environments.

The pilot area is located near Beaume-les-Dames, in the French department of Doubs (Figure 14). It is a sparsely developed rural sector with mainly fields used for cattle grazing. The local geology is dominated by oolitic and crinoidal limestones of Middle Jurassic age (Bathonian and Bajocian). The sector is crossed by numerous faults on a north-south axis. It shows numerous signs of a karst environment: alignments of sinkholes, losing stream and resurgences, numerous underground cavities… A cavity with an underground river crosses the study area. The cavity and the underground river are accessible via a drilled well and have been instrumented for several years by the University of Franche-Comté, located in Besancon.

As part of this study, the content of natural radionuclides in soil and rock was determined as well as the permeability of the soils. Continuous measurements of radon-222 volumetric activities in the air of the underground cavity were carried out over a period of one year, from October 28, 2015 to December 7, 2016. Continuous measurements of radon-222 activity concentrations in the soil air directly above the cavity were carried out at various measuring points during the same measurement period. In addition, meteorological parameters were recorded by a weather station located near the measuring points.

Thanks to a post-doctoral contract funded by the European RadoNorm project, new data were acquired in the laboratory: measurements of density and measurements of emanation coefficient ε from rocks and soils taken from the study area.

These new data can be added to the data already acquired in order to complete the numerical model of radon transfer to the surface.

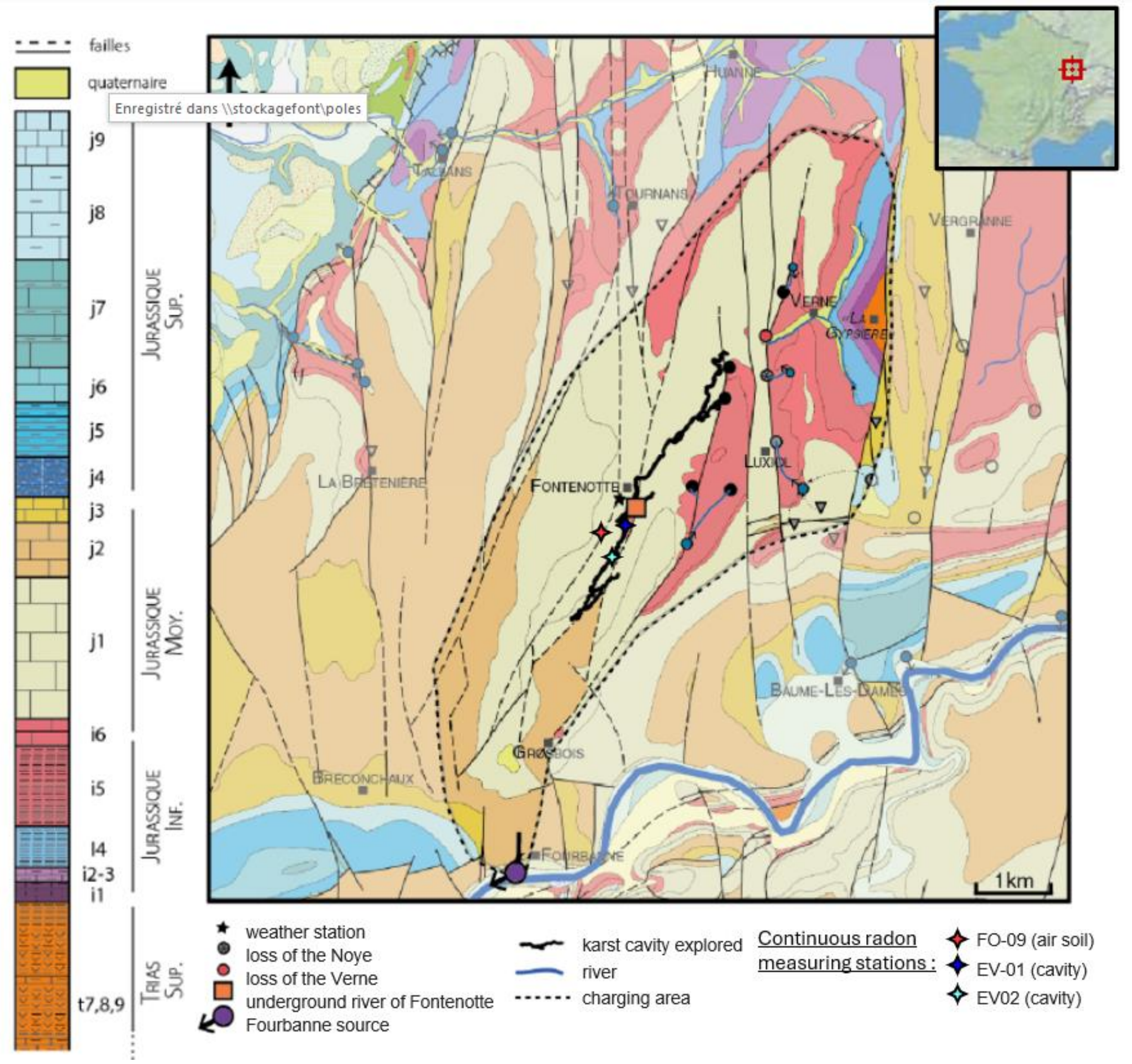

Figure 14 - Location of the study area and measurement points on the geological map at scale 1/50,000 adapted from [43].

2.3.2 Data Description

2.3.2.1 Characterization of soils and rocks

At the measurement point FO-09, a soil sample was taken with an auger at a depth of 50 cm. Limestone blocks were taken from the walls of the cavity (samples called FR-02 and FR-03).

The mass activity of Ra-226 and U-238 in soil and rocks are measured by gamma spectrometry. For each sample, the Ra-226 content is derived from the Pb-214 measurement, and the U-238 content from the Th-234 measurement. The results are shown in Table 15.

Table 15 - Results of radium-226 and uranium-238 activity measurements for FO-09 soil sample and for limestone samples

Sample name	Sample type	Ra-226 activity (Bq/kg)	Uncertainty (k = 2)	U-238 activity (Bq/kg)	Uncertainty (k = 2)
FO-09	soil	83	8	< 24	
FR-02	limestone	18	2	17	11
FR-03	limestone	12	1	14	10

Soil gas permeability was measured using a RADON-JOK device, developed by RADON v.o.s. It enables in-situ measurement of soil gas permeability by means of negative pressure air suction [44]. Soil gas is pumped at constant pressure, using weights, through a sampling tube sunk into the soil and connected to a two-litre bellows previously emptied of air. Considering a homogeneous soil, soil gas permeability is calculated on the basis of Darcy's equation. It is therefore determined from the rate at which air is extracted from the soil through the sampling tube, and hence the time required to fill the bellows, according to the following formula:

$$Q = F \ \frac{k}{\mu} \ \Delta p \qquad (1)$$

With *Q*, the air flow (m^3/s), *F*, probe form factor (m), *k*, soil gas permeability (m^2), *μ*, viscosity (Pa.s) and *Δp*, the pressure difference between the surface and the active area of the probe (Pa)

The results of the permeability measurement carried out at site FO-09 are presented in *Table 16 -* .

Table 16 - Results of soil air permeability measurement in FO-09 location (measurement performed on 01/07/2015) and moisture content measurement

Measurement location	Permeability (m^2)	Uncertainty (k=2)
FO-09	1,15E-12	1,71E-13

For the analysis of the particle size distribution of soil samples, the mass fractions of the different average diameters of solid soil particles are determined using a particle size analyser. The results of the particle size distribution measurement for FO-09 soil sample are presented in *Table 17 -* .

Table 17 - Soil particle size class of site FO-09

Particle size class	Grain size [%]
Clay	42.45
Fine silt	32.14
Coarse silt	17.61
Fine sand	2.99
Coarse sand	4.82

2.3.2.2 Continuous measurements of radon

Continuous measurements of radon-222 levels were carried out in the soil and in the cavity for more than a year, from the end of October 2015 to the beginning of December 2016. The measurements were carried out using a BMC2 type measuring probe (in accordance with the requirements of standard NF ISO 11665-5).

The measurement of the radon isotope 222 is carried out using a silicon detector placed in a closed enclosure protected by filters. The presence of a dead volume located at the entrance of the probe makes it possible to do without the radon isotope 220. Powered by an alkaline battery box, it is designed to measure radon concentrations ranging from a few hundred Bq.m^{-3} to 10^{9} Bq.m^{-3} with an autonomy of around one year. Its design allows it to withstand difficult atmospheric conditions (high humidity, high temperatures). The BMC2 probe performs a simultaneous measurement of radon as well as temperature and atmospheric pressure.

In the soil, the BMC2 probe was installed at a depth of 1 m, in a PVC tube (FO-09). Figure 15 shows the evolution of the radon levels recorded continuously during the study period in soil. Radon levels range from 28 kBq/m^3 to 121 kBq/m^3 with an average of 73 kBq/m^3 recorded over the measurement period.

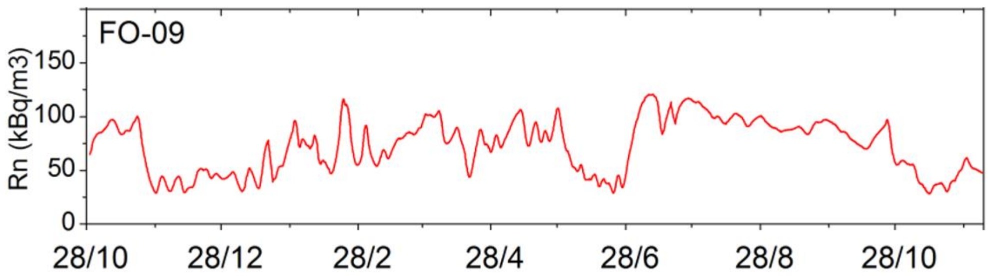

Figure 15 - Continuous measurements of radon-222 activity in soil air recorded from October 28, 2015 to December 7, 2016 with BMC2 probe (values smoothed with a 48-hour floating average)

Two probes were also installed in the underground cavity to measure the ambient air (EV-01 and EV-02). Figure 16 shows the evolution of the radon-222 levels recorded continuously during the study period in the cavity. The two probes are about 500 meters apart. Radon-222 levels range from around 100 Bq/m^3 to 15,000 Bq/m^3 with an average of 3,500 Bq/m^3 recorded over the measurement period.

These measurements confirm that the radon volumetric activity is relatively homogeneous in the cavity, the orders of magnitude and the variations observed being similar at the two stations. The minimum values are observed in winter and the maximum values are observed in summer, from June to September.

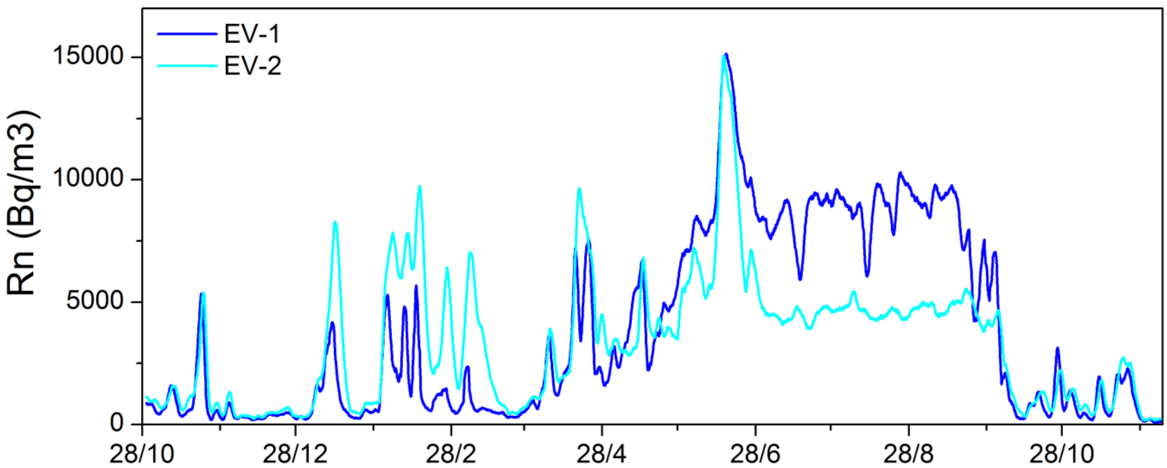

Figure 16 - Volumetric activity of radon-222 recorded from October 28, 2015 to December 6, 2016 in the En Versenne cavity at the two measuring stations (values smoothed with a 48-hour floating average)

2.3.3 Data Analysis

2.3.3.1 New measurements

2.3.3.1.1 Determination of emanation coefficient factor ε

The measurement of the emanation coefficients of soil and rock samples was carried out within the framework of a post-doctoral contract funded by the European RadoNorm programme. The protocol followed is described in the article [45].

The emanation coefficient ε is calculated by the measurement of the effective radium-226 concentration, εCRa. This is the product of radium-226 activity concentration *CRa* (previously measured by gamma spectrometry) and the dimensionless quantity ε, which is the probability that after radioactive decay, the daughter radon-222 atom is released in the pore space of the medium, from where it can be subsequently transported to the environment. Thus, in the case of radium-226, in the uranium-238 decay chain, εCRa is the natural source term of radon-222.

In their article, Girault and Perrier [45] explain a procedure for measuring the effective concentration of radium with large number of samples simultaneously by the accumulation method with scintillation flask and alpha counting.

Bottles with narrow throats are used for the purpose, and these are closed using a pre-perforated natural rubber stopper, which ensured excellent airtightness. At first, accumulation experiments were performed with empty vessels to check any possible contamination in the glass bottles. No significant counts were seen for air sampled from these empty glass bottles. Once the sample were added, the glass container was closed. After the accumulation time (which varied from 1 – 20 days), air from the vessel was sampled into a ZnS(Ag) scintillation flask previously evacuated to a pressure varying between 10 and 20 mbar. Pressure was measured using a digital manometer in the container before sampling, and again in the flask after transfer. For the transfer, syringe needles were used with a valve and a 0.45 mm cellulose filter to prevent radon-222 decay products from entering the scintillation flask. The sampled flask is then placed for a resting time of about 3 h, necessary for radon-222 to reach equilibrium with its decay products. This delay would also ensure radon-220 elimination. Later the scintillation flask was inserted in a photomultiplier for alpha counting. Each flask was counted two times for five minutes each. From the observed average count, the previously measured mean flask background was subtracted. The radon-222 concentration, expressed in Bq/m^3, was then calculated.

From the value of the radon-222 concentration C_{Rn}, the value of εC_{Ra} is deducted with the following formula:

$$\varepsilon C_{Ra} = \frac{V_a}{m} \frac{C_{Rn}}{1 - e^{-\lambda t}} \quad (2)$$

With V_a, the free air volume in the bottle, m, the mass of the sample, λ, the decay constant of radon-222 (2.1×10^{-6} s^{-1}) and t, the accumulation time (between 1 and 20 days).

Accumulation experiments were repeated several times, with different accumulation times. The curves obtained for the different samples measured in this study are visible in Figure 17.

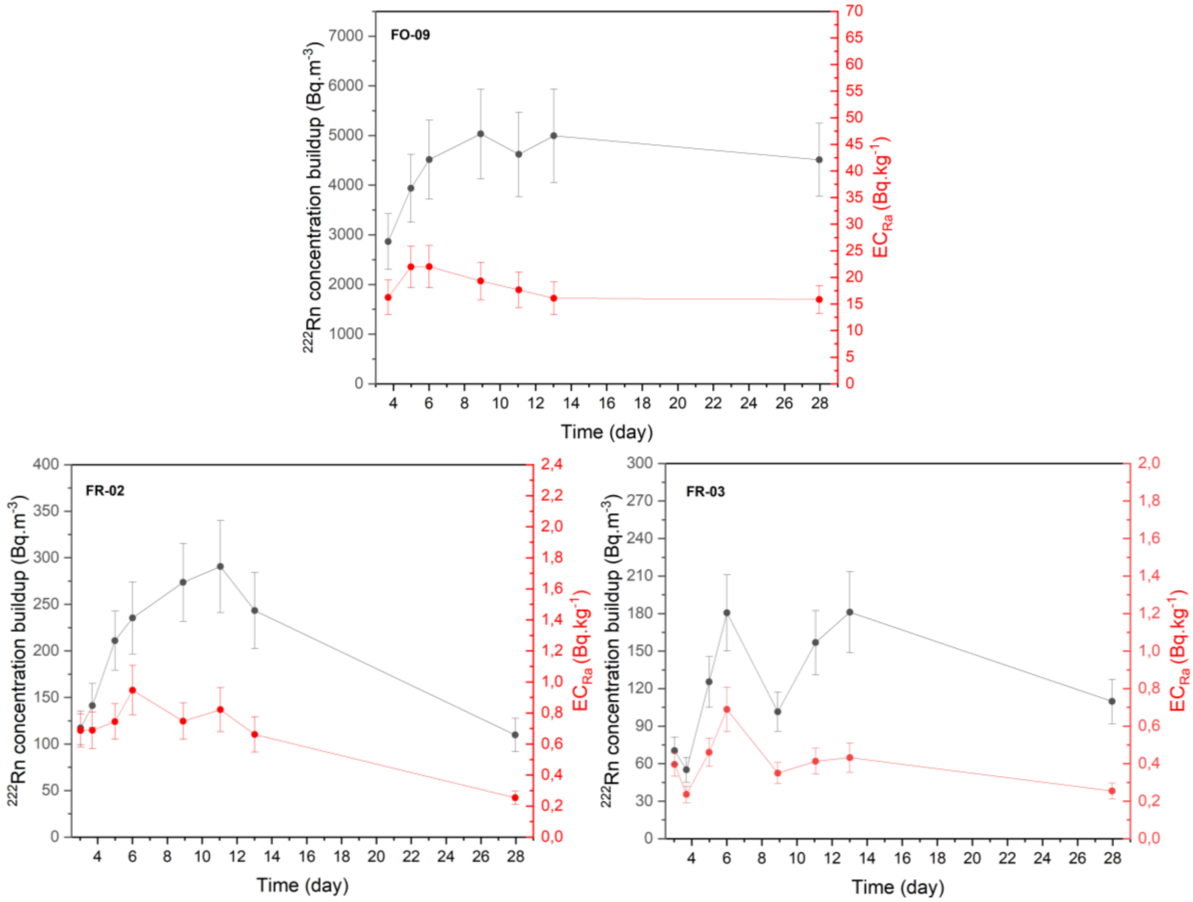

Figure 17- Rn-222 concentration and εC_{Ra} buildup curve for FO-09 soil sample and rock samples FR-03 and FR-02

The final value of εC_{Ra} is calculated by averaging the different values of εC_{Ra} obtained and the coefficient ε is deduced from the C_{Ra} data acquired by gamma spectrometry. The results are in **Fehler! Verweisquelle konnte nicht gefunden werden.**.

Table 18 - Estimated values of radon-222 emanation factor for soil and rock samples using alpha counting methods

Sample ID	Alpha counting method				
	εC_{Ra} (Bq kg^{-1})	C_{Ra} (Bq kg^{-1})	ε	DF*= (DF1~DF2)/2	%ge DF* > σEC$_{Ra}$] (%)
FO-09 (soil)	18.4 ± 5.4	83 ± 8	0.22 ± 0.1	0.0974	3
FR-02 (rock)	0.74 ± 0.11	18 ± 1	0.04 ± 0.002	0.1604	> 10
FR-03 (rock)	0.43 ± 0.15	12 ± 1	0.04 ± 0.001	0.1067	> 10

2.3.3.1.2 Grain density measurements

The grain density of rock and soil of the study site was measured by helium pycnometry technique [46]. Gas pycnometry is a widely used gas displacement-based analytical technique for precise volume measurements. The displacement media are usually inert gases. After the sample is sealed inside a known volume instrument compartment and a proper inert gas is introduced, it is expanded into a second precision internal volume. The pressure before and after expansion is measured and used to compute the sample volume. Gas displacement density is then obtained by dividing this volume by the sample weight. The AccuPyc II 1340 Pycnometer (Micromeritics France S.A, France) is a fast, fully automated system that provides high-speed, high-precision volume measurements and density calculations on a wide variety of powders, solids, and slurries having volumes from 0.01 to 350 cm^3. Data collection, calculations and displaying the results are done by the instrument uninterrupted, at every analysis cycle.

The result obtained for the soil sample FO-09 is in the **Fehler! Verweisquelle konnte nicht gefunden werden.**.

Table 19 - Grain density values measured using He pycnometer

Sample ID	$M_{ech}(Kg)$	$\rho\ (Kg\ m^{-3})$
FO-09 (soil)	0.00368	2,556.7 ± 3.3

2.3.3.2 Modelling

2.3.3.2.1 Model description

Numerical modelling can be used to understand the phenomena involved in the radon transport and variability in the karstic system and to explain the conditions leading to high radon concentrations in soils. Therefore, a model of radon transport from the caves to the soil surface was developed and calibrated with the experimental data. This model used a simplified Brinkman modelling approach, allowing two-phase flow through a transition zone created at the interface between the cave and the limestone rock, in order to ensure the gradual transition of physical properties such as porosity and permeability. The numerical modelling was performed using the T2Rn code developed at ASNR (formerly IRSN) based on the iTOUGH2 platform (transport of unsaturated groundwater and heat) in collaboration with LBNL (Lawrence Berkeley National Laboratory, Berkeley, California-USA) [47]. To have a realistic model, several parameters were needed: (i) geometrical characteristics of domain, (ii) physical hydrodynamic properties, soil radon source and transport properties, (iv) initial conditions, and (v) boundary conditions. According to the availability of meteorological data, the measurement period from 20/04/2016 to 25/05/2016 were selected. **Fehler! Verweisquelle konnte nicht gefunden werden.** shows the meteorological parameters averaged over this period.

Table 20 - Mean meteorological parameters for the studied period

Atmospheric air temperature, T_{atm} [°C]	**10.07**
Atmospheric air pressure, P_{atm} [Pa]	9.7024 E+04
Potential evapotranspiration, ETP [mm]	1.29
Rainfall, R [mm]	180.2

2.3.3.2.2 First model: Influence of meteorological variations (atmospheric air pressure and rainfall) and mass activities of radium-226

Weather conditions have a significant influence on the transport of radon in soil. The most important meteorological factors are rainfall and the soil air pressure. In order to distinguish their respective influence, a simplified configuration was considered (Figure 18). In this configuration: (i) only the soil was considered (the cavity is omitted), (ii) the soil is assumed to be homogeneous (silty clay), the domain is assumed to be infinite in order to eliminate the effect of the lower boundary condition, and (iv) the only source of radon is its generation by emanation from the zone containing radium-226 (this zone is delimited by the red line in Figure 18). The parameters used in these simulations are shown in **Fehler! Verweisquelle konnte nicht gefunden werden.**.

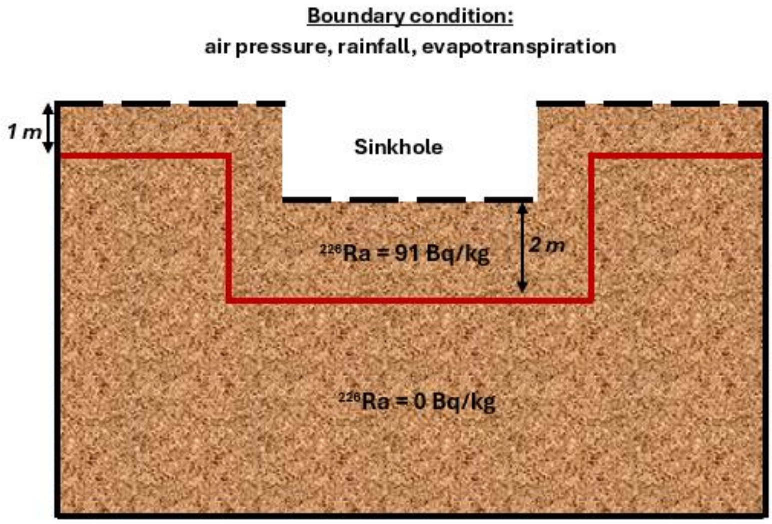

Figure 18 - Schematic representation of the simplified domain (infinite homogeneous medium)

Table 21 - Parameters used (simplified domain)

Emanation coefficient (-)	Bulk density (Kg/m³)	Radium-226 mass activity	Porosity ϕ (-)	Permeability (m²)	Van -Genuchten model parameters	
					α_{VG} [cm^{-1}]	m_{VG}
0.22	2556.7	91	0.5	3.46 E-12	0.020	0.157

The model reproduces trends in measured radon-222 activity volumes (**Fehler! Verweisquelle konnte nicht gefunden werden.**). With the parameters used, the modelled radon-222 levels in soil air modelled are close to those measured. According to this simulation, the average radon-222 activity levels measured in the soil correspond to those calculated by simple emanation and diffusion in the soil layer, taking into account the radium-226 content measured in the soil. Radon-222 volumetric activity peaks and their durations are reproduced by the T2Rn code. However, the intensities of the calculated peaks are lower and decrease more rapidly than the measured peaks.

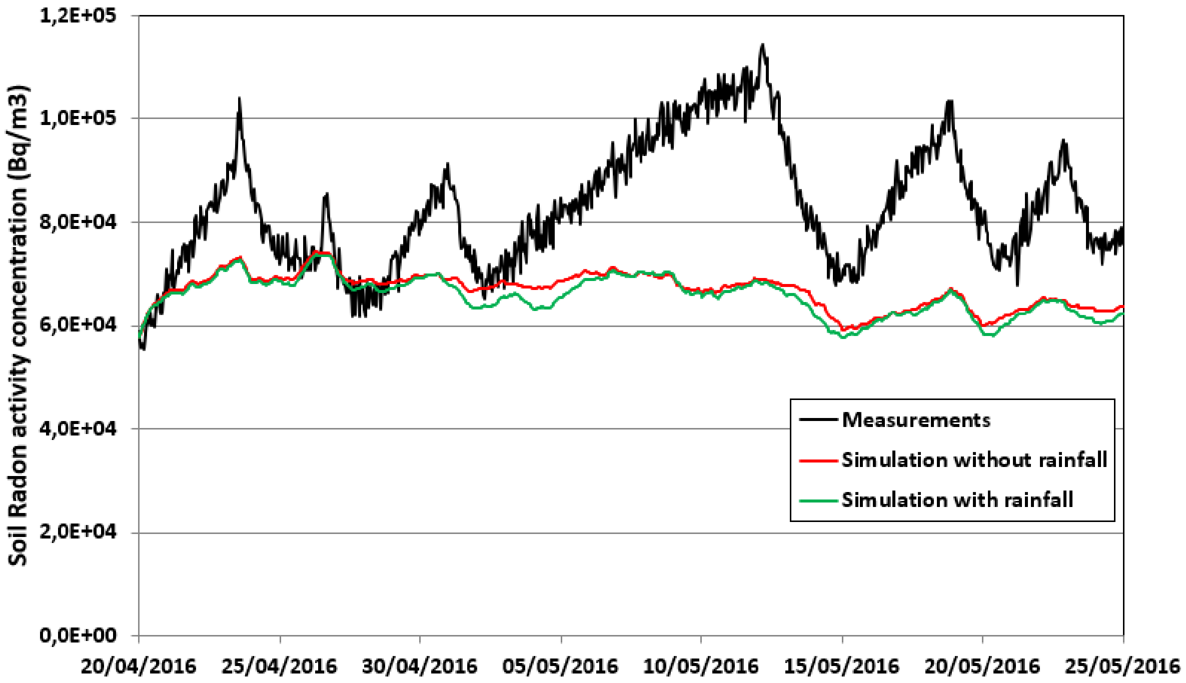

Figure 19 - Evolution of radon activity in soil air measured and calculated by the T2Rn code with and without rainfall. Calculations performed for a simplified domain.

2.3.3.2.3 Second model: Influence of air pressure and radon volumetric activity in the cavity

In the second configuration (**Fehler! Verweisquelle konnte nicht gefunden werden.**20), the complete domain was modelled. The goal of this configuration is to quantify the impact of the cavity. However, karst systems are complex to model due to the combined effects of nonlinearity and heterogeneity, which result from the geological media, cave systems, and their spatial variability. For this, a transition zone was created at the interface between the cave and the limestone rock using a simplified Brinkman modelling approach, to ensure the gradual transition of physical properties such as porosity and permeability.

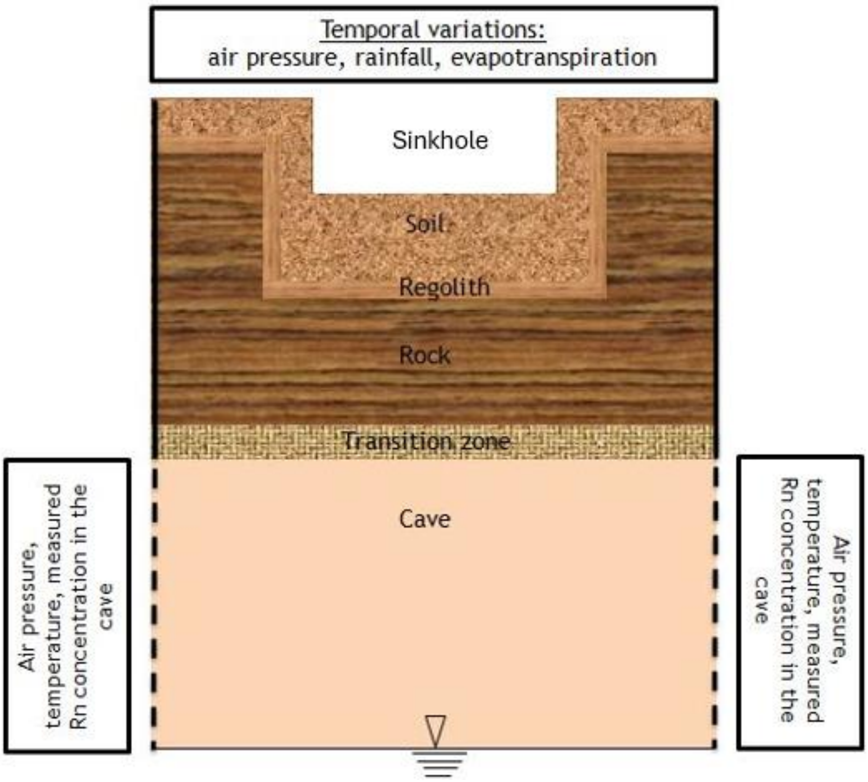

Figure 20 - Schematic representation of the complete domain

The computational domain (**Fehler! Verweisquelle konnte nicht gefunden werden.**) consists of a cavity, treated as an open medium, and four layers: soil, regolith, rock, and a transition zone. The parameters of this domain are presented in **Fehler! Verweisquelle konnte nicht gefunden werden.**. The length and depth of the sinkhole, formed by limestone dissolution, are estimated based on topographic surveys conducted by ASNR (formerly IRSN) during field missions. For this model, the following assumptions are made: (i) the sinkhole and cavity are considered rectangular, (ii) the soil thickness is estimated to be 2 meters at the bottom of the sinkhole and 1 meter at its edges, the cavity height is assumed to be equal to the diameter of the Fontenotte chamber in the En Versenne cave (i.e. 16 m), and (iv) the thickness of the transition zone is chosen based on the physical and hydrodynamic properties of the rock and cavity (i.e. 0.3 m).

Table 22 - Parameters used (complete domain)

Layer	Emanation coefficient (-)	Porosity ϕ (-)	Permeability (m²)	Van -Genuchten model parameters	
				$\alpha_{VG}\ [cm^{-1}]$	m_{VG}
Soil	*0.22*	*0.5*	3.46 E-12	*0.020*	*0.157*
Regolith	*0.25*	*0.36*	6.92 E-12	*0.020*	*0.157*
Rock	*0.25*	*0.01*	6.80 E-10	*0.010*	*0.150*
Transition zone	*0.25*	$0.01 < \phi < 1$	$6.80\ \text{E}-10 < k < 1.0\ \text{E}-08$	*[0.01 - 0.10]*	*[0.150- 0.195]*
Cavity	-	*1*	1.0 E-08	*0.1*	*0.195*

The results (**Fehler! Verweisquelle konnte nicht gefunden werden.**) showed that the amplitudes of the radon-222 activity fluctuations in the soil air are related to the pressure gradients in the soil caused by the pressure fluctuations in the cavity. Moreover, the average levels of radon-222 activity in the soil are mainly the result of its generation by emanation from the radium-226 contained in the soil.

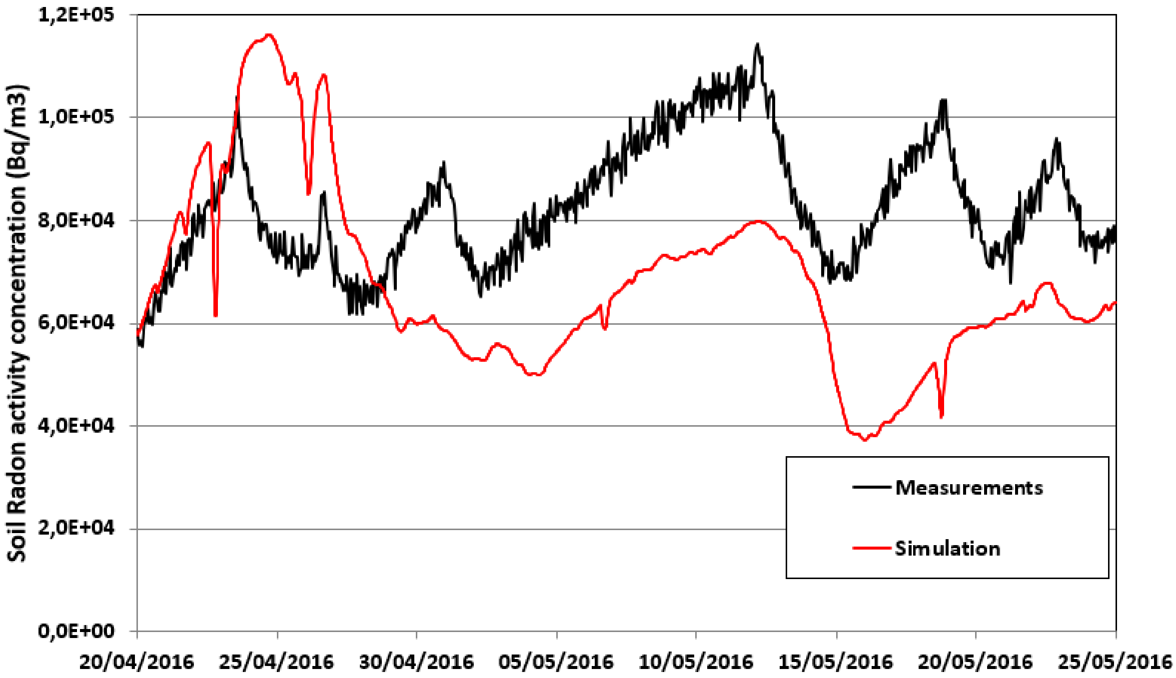

Figure 21 - Evolution of radon-222 activity in soil air measured and calculated by the T2Rn code – calculations performed for a complete domain.

2.3.4 Results

This study confirmed that karstic environments could be the source of locally high radon-222 contents in the soil. However, a high variability of radon-222, both spatial and temporal, was observed in the soils of the study area.

The numerical model of radon-222 transfer to the surface shows that the average radon-222 activity levels in the soil are mainly the result of radium-226 emanation from the soil. Fluctuations in radon volume activity observed in the soil appear to be related to the existence of pressure gradients from the cave to the ground generated by pressure variations in the cave. According to the model, it is the presence of the underlying cavity that explains the temporal variability of radon-222 in the soil air and the occasional very high values.

2.4 Italian Analysis

2.4.1 Introduction

The analysis performed on the two combined Italian datasets (2.4.2) (voids and radon concentration measurements) aims to evaluate potential correlations between the radon concentration in dwellings above voids and their distance from the void centres, within a 100-meter range.

For this purpose, we defined concentric circles around each void's centre with radii in 10-meter increments (Figure 22), forming annular regions. We then calculated the mean radon concentration for all dwellings within each annular region.

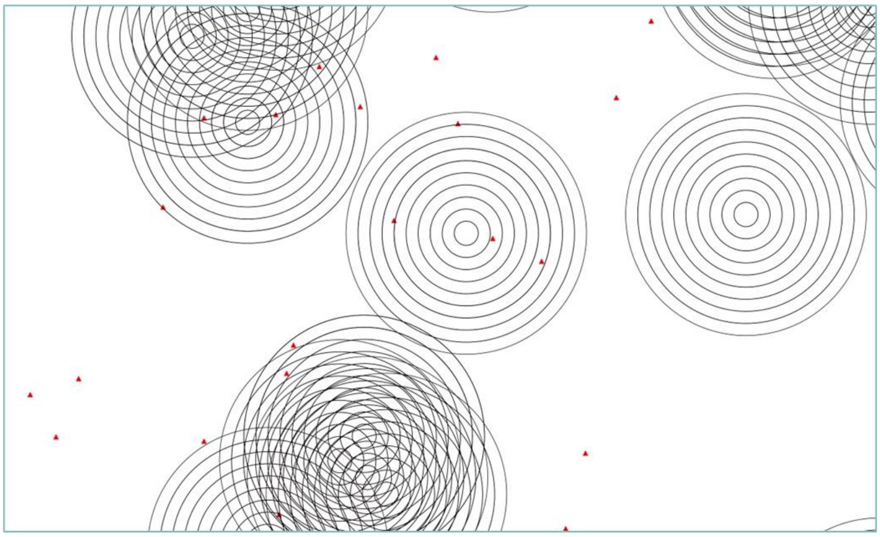

Figure 22 - Concentric circles around void's centres and position of dwellings with radon concentration (red triangles)

2.4.2 Data Description

The Italian available datasets consist of two different datasets, one on Rome Municipality's voids and the other on IRC measurements from an epidemiological survey of 2010 conducted in the city of Rome.

Datasets on voids characteristic

This dataset is made up of 3057 entries in GIS format (a geographical information system) i.e. a format containing geospatial data, provided by the Rome Municipality. In this database we have the position of different types of voids located in the city of Rome, but no information on radon concentration inside the voids. The voids in the database are described in Table 23.

Dataset on radon concentration measurements

This dataset has 1441 entries (measurements of radon concentration in 1441 dwellings) from a survey of 2010 in the Rome Municipality. The dataset description is reported in Table 24.

Table 23 - Types of voids

Type of Voids	# of Voids
Bunker	308
Catacomb	90
Cavity found in survey	1596
Tunnel	335
Fortress	15
Entrance to quarry	670
Isolated Hypogeum	43

Dataset on radon concentration measurements

This dataset has 1441 entries (measurements of radon concentration in 1441 dwellings) from a survey of 2010 in the Rome Municipality. The dataset description is reported in Table 24.

Table 24 - Description of the dataset on radon concentration measurements in City of Rome (2010)

Dataset Variables	Description of variable
Region	Lazio
ID_Survey	Identify the survey
ID_Dwelling	Unique identifier for dwelling
City	Rome
Geographical address	Address of dwelling
Building number	Street number of dwelling
Floor	Floor of dwelling
Annual mean radon concentration (Bq/m^3)	Value of mean radon concentration in dwelling in Bq/m^3
Longitude	Dwelling's geographical coordinate for longitude in decimal format
Latitude	Dwelling's geographical coordinate for latitude in decimal format
Address from geocoding	This is the address from latitude and longitude geocoding to compare with geographical address for dwelling

The last variable, “Address from geocoding”, of the above dataset (on radon concentration measurements in dwellings) allows us to check if the geographical coordinates are correct. In fact, by a geocoding tool, we can obtain a geographical address from geographical coordinates and then compare this one to the “Geographical address” variable value.

By merging the positions of voids and dwellings using the QGIS tool we generated the map in Figure 23.

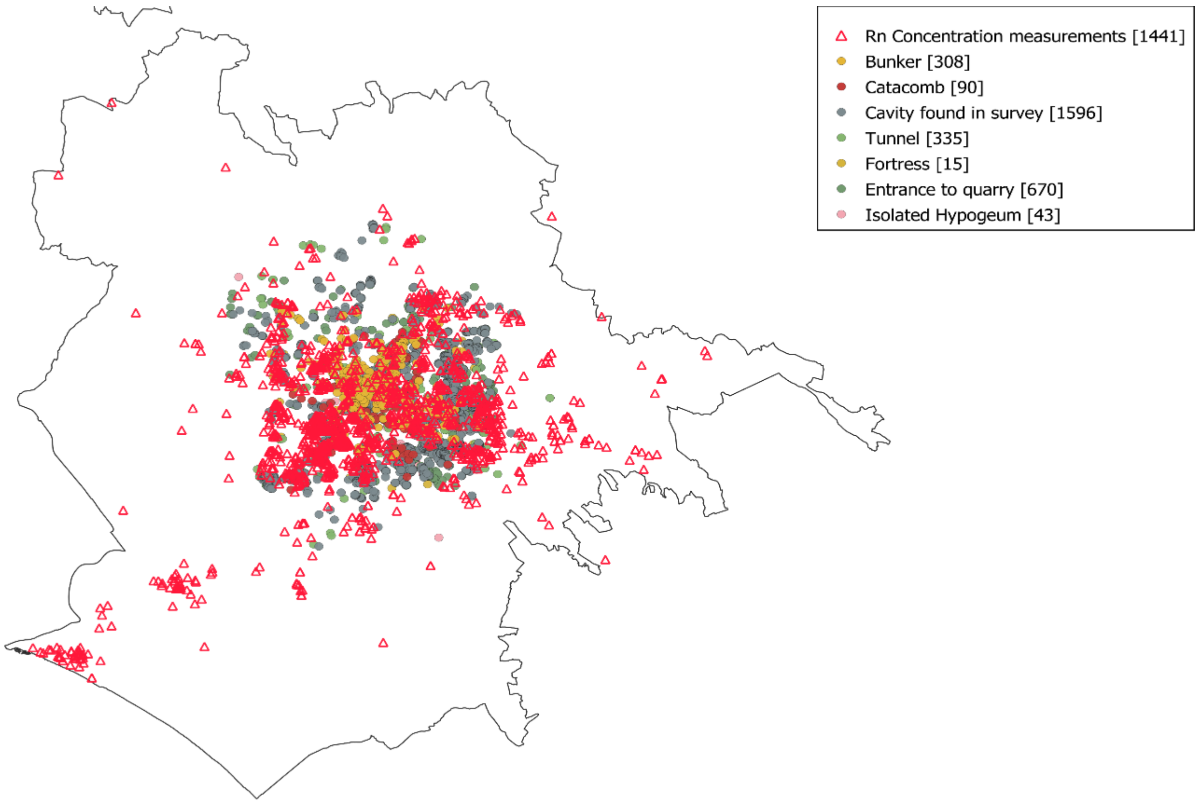

Figure 23 - Spatial distribution of voids of different types and IRC measurement positions

2.4.3 Analysis Description

From the initial 1,441 measurements, the dataset was reduced to 653 by excluding measurements beyond 100 meters from void centres. After removing 19 measurements lacking floor information, 634 remained. To avoid interference effects from multiple voids on a single dwelling, we considered only the void nearest to each dwelling's position, further reducing the sample size to 277 measurements.

Using QGIS software, we overlaid the voids (with their defined rings) and radon concentration measurement position (277) to generate a table showing mean radon concentration within each annular region.

2.4.4 Results

In Table 25 are presented the results of the overlap of voids and radon concentration measurements, where Ring ID (multiplied by 10) indicates the distance in meters from void centres, and “counts” show how many dwellings are located within the annular region. Figure 24 displays the mean radon concentration versus distance from void centres including also standard error (SE) bars. As evident from Figure 24, this analysis reveals not significant variations in mean radon concentration relative to distance from the void centres.

Table 25 - Mean concentration value versus distance from void centre (indicated as Ring ID)

Ring ID	Mean	SE	Counts
1	76	14	11
2	84	19	12
3	117	23	28
4	99	15	20
5	90	11	32
6	107	11	44
7	100	9	31
8	105	9	39
9	97	10	31
10	114	21	29

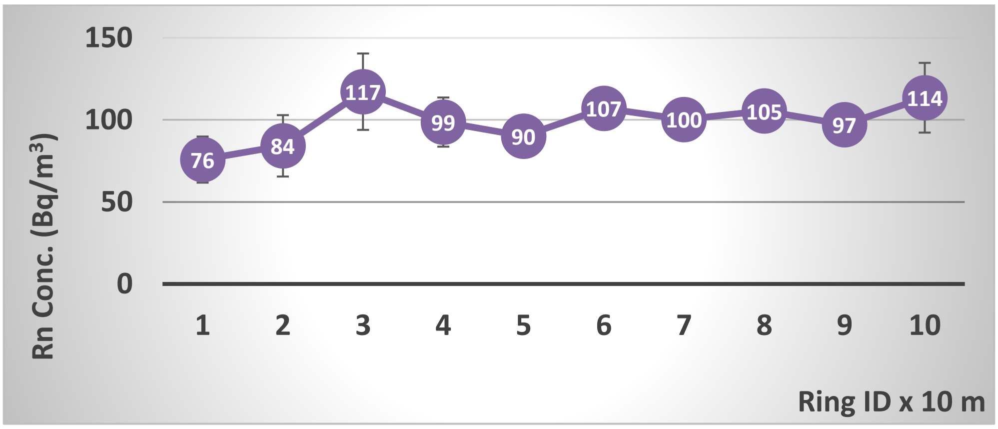

Figure 24 - Mean (with Standard Error) radon concentration versus distance from void’s centre.

To further investigate this relationship, we conducted an additional analysis using also the information on the dwelling floor, stratifying the data into three categories based on measurement floor.

Table 26 presents the analysed data for the three floors and each annular region, including Ring ID, mean radon concentration, standard deviation, and measurement counts per region.

The mean radon concentrations versus Ring ID across three different floors are compared in Figure 25. Two values stand out as significantly different: Ring ID 2 for ground and Ring ID 3 for first floor measurements. However, these results require further investigation due to limited data - Ring ID 2 has only one entry and Ring ID 3 for the first floor includes six entries but with different void types. For these reasons additional analysis is needed with larger sample sizes and stratification by void type to validate these findings.

Table 26 - Mean radon concentration value versus distance from void centre (indicated as Ring ID) for the three different floors of the dwellings analysed.

	Floor								
	All > First			First			Ground		
Ring ID	**Mean**	**SE**	**Counts**	**Mean**	**SE**	**Counts**	**Mean**	**SE**	**Counts**
1	76	21	6	75	21	5			0
2	67	10	9	67	27	2	269	70	1
3	100	28	16	191	77	6	90	13	6
4	110	24	12	74	14	5	95	16	3
5	74	8	19	109	24	11	140	100	2
6	100	12	28	114	24	8	125	33	8
7	97	12	19	91	9	8	134	32	4
8	106	12	24	103	19	9	108	15	6
9	99	12	21	71	15	6	126	32	4
10	113	30	20	104	34	4	123	27	5

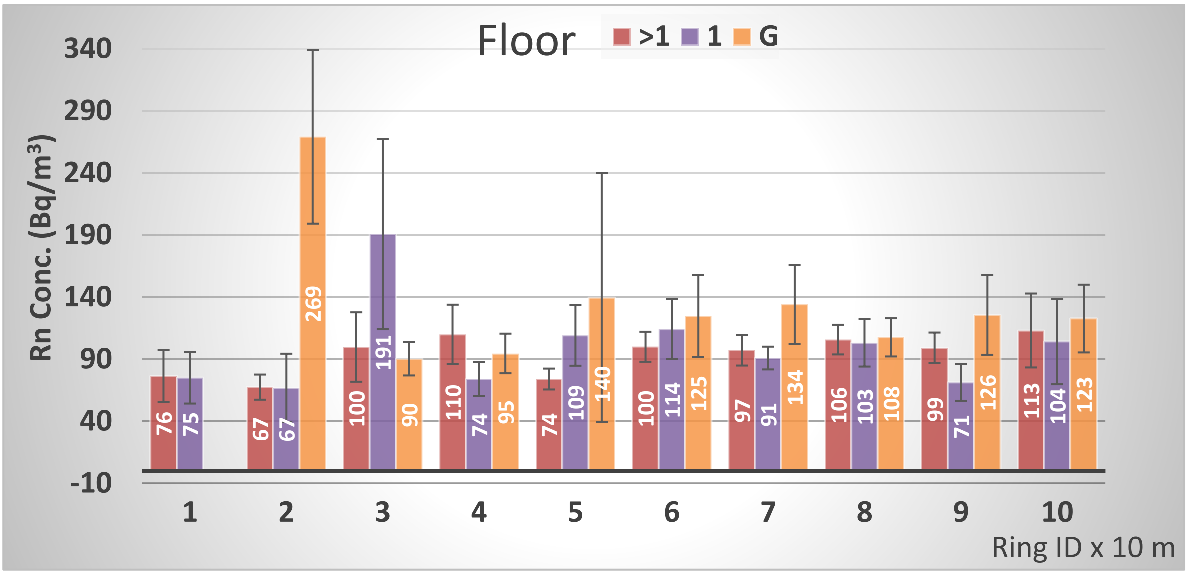

Figure 25 - Mean radon concentration versus distance from void's centre (with Standard Error) for different floors.

The primary conclusion of this preliminary analysis is that no significant variations in mean radon concentration were observed relative to the distance from the void centres. This suggests that, at a general level, the proximity to the studied urban voids (bunkers, catacombs, cavities found in surveys, tunnels, fortresses, entrances to quarries, isolated hypogea) does not have a widespread and directly proportional impact on indoor radon levels in the dwellings above them.

Further investigations that consider the floor level of the dwellings highlighted two instances of potentially significant differences in mean radon concentrations at specific distances (Ring ID 2 for ground floor and Ring ID 3 for the first floor). However, these results require further investigation due to the limited number of data points in those specific distance ranges and the mixture of different void types within them.

Therefore, the Italian analysis concludes that additional research with larger sample sizes and a stratification of the analysis by void type is needed to validate these initial findings and to gain a more detailed understanding of any potential specific relationships between certain types of urban voids and IRC.

In essence, while the initial analysis did not find a general correlation, specific cases warrant further scrutiny with more refined data and analysis methods.

2.5 Swiss Analysis

2.5.1 Introduction

In Switzerland, radon exposure is a recognized public health issue, contributing to an estimated 200–300 lung cancer deaths annually [48]. The Federal Office of Public Health (FOPH) handled the topic at the national levels and implemented various measures to address this risk, highlighting the need for effective mitigation strategies. Switzerland's complex alpine geology significantly influences radon distribution, as the geological characteristics vary greatly between regions.

Within Switzerland’s diverse geological landscape, the Jura and Prealps regions contain extensive karstic formations. Although these rocks are not uranium-rich, they are considered radon-prone areas, as depicted by in-site IRC measurements [49]. According to the current state of arts, there remains significant uncertainty and a general lack of understanding regarding the influence of karst voids on IRC. Therefore, it is essential to investigate in greater detail the impact of specific factors, such as the composition of the geological layers, the proximity to karstic faults, and the presence of underlying karst networks. These different elements may play a critical role in determining radon concentrations and this work is aiming to assess their relative influence on IRC.

2.5.2 Dataset description

This study serves as a preliminary investigation aimed at identifying general trends, which will be analysed in greater detail in subsequent research phases.

The study is based on the Swiss radon database provided by the Federal Office of Public Health (FOPH). This database contains approximately 250,000 radon measurements collected from 150,000 buildings across the inhabited areas of Switzerland, as in its state in December 2020. All measurements are georeferenced, enabling spatial analysis and integration with additional datasets. Using the georeferenced radon data, information from several GIS datasets was attributed to each radon measurement. Table 27 summarises the origin and sources of the various datasets incorporated into this analysis.

Several filters were applied to the dataset. First, only measurements conducted from 2005 (a maximum of 20 years old) were included in the analysis. Second, only measurements carried out on the ground floor, -1 level and -2 level were considered.

Table 27 - Descriptions, sources, and references of the different dataset included in the predictive analyses [50].

Thematic	Source	Data type	Availability	Version	Variables	Description	Extent and resolution	Reference
Radon	FOPH	Data-base	On request	December 2020	- Indoor radon levels - Building type - Building characteristics (age, floor, foundations) - Geographical coordinates	National indoor radon measurements database. Each measurement is geo-localised and referenced with the EGID of the building.	Not applicable	Not applicable
Radon	FOPH	Raster	Open-source	June 2017	- Spatial probability.	Probability map of exceeding the national radon reference level (300 Bq/m^3).	Switzerland, 1 x 1 km	[49]
Geology	Swisstopo	Vector	Open-source	Version 1.3, June 2014	- Geological class - Lithology class - Great geological areas - Rock type - Area - Genese - Cover - Faults	GIS file (Shape file) containing different geological layers. Vectorial layers correspond to the data contained in the 1:500000 geological maps of Switzerland.	Switzerland, vectorial layers	[51]
Uranium	FOEN	Raster	Open-source	December 2023	- Concentration of uranium in the soil (mg/kg of fine earth)	Raster layer representing an interpolation (kriging method) of uranium concentration in soils, issued from the Geochemical soil atlas of Switzerland.	Switzerland, 1 x 1 km	[52,53]
Seismic risk zone	FOEN	Vector	Open-source	March 2011	- Seismic risk classification	Vector data mapping the different risk classes of seismic activity	Switzerland, vectorial layer	[54]

Thematic	Source	Data type	Availability	Version	Variables	Description	Extent and resolution	Reference
Ecological and forest (ecoforest) regions	FOEN, WSL	Vector	Open-source	June 2020	- Delimitation of ecoregions	Vector layer presenting the delimitation of the forest ecoregions.	Switzerland, vectorial layer	[55]
Climatology	MeteoSwiss	Raster	Open-source	2021	- Temperature - Solar irradiance - Precipitation	Raster layers representing the annual mean temperature, mean Solar irradiance and sum of precipitation for the period 1991 – 2020.	Switzerland, 1 x 1 km	[56]
Karstic catchments	FOEN	Vector	Open-source	2016	- Area - Name - Surface	Delimitation and properties of Switzer-land's karstic catchments	Switzerland, vectorial layer	[57]

2.5.3 Analysis Description

The analyses conducted in this study consist of comparative analyses based on various parameters. Comparative tables and figures are presented to identify potential influences of karst networks on indoor radon levels.

2.5.4 Results

Figure 26 illustrates IRC across Switzerland categorized by the main rock types. At the national level, the highest IRC were recorded in regions with igneous rocks, particularly in granite massifs such as Mont Blanc, Aar, and Bernina. These are followed by radon levels recorded in areas with sedimentary rock formations. Figure 27 presents the same dataset as Figure 26, with additional consideration of the building levels where radon measurements were conducted. The overall trends remain consistent, with the highest radon concentrations observed in igneous rock regions. These are followed by measurements in sedimentary rock areas on ground floors and in metamorphic rock areas at basement levels (-1 and -2).

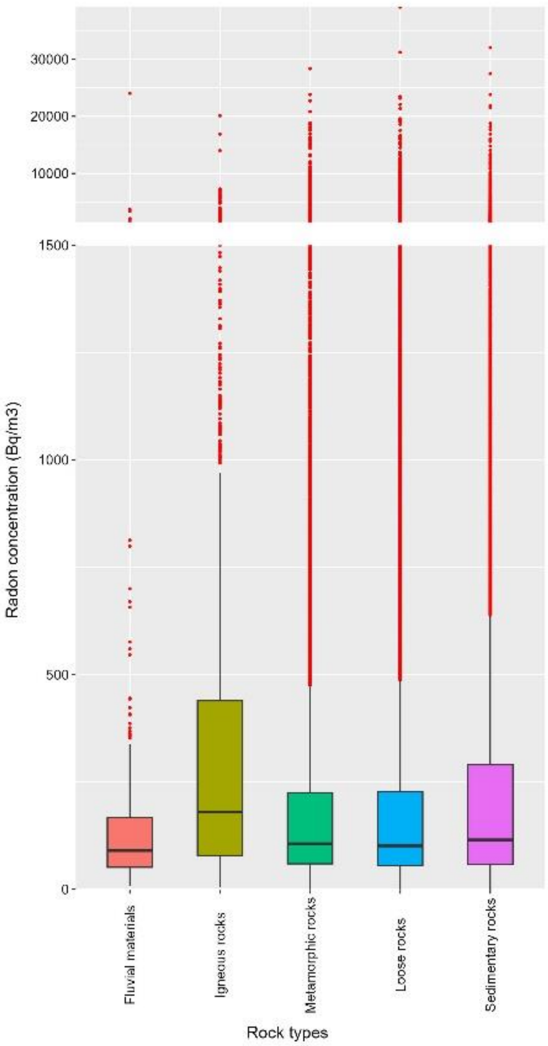

Figure 26 - Boxplot distributions of IRC relative to the underlying rock type at the national scale.

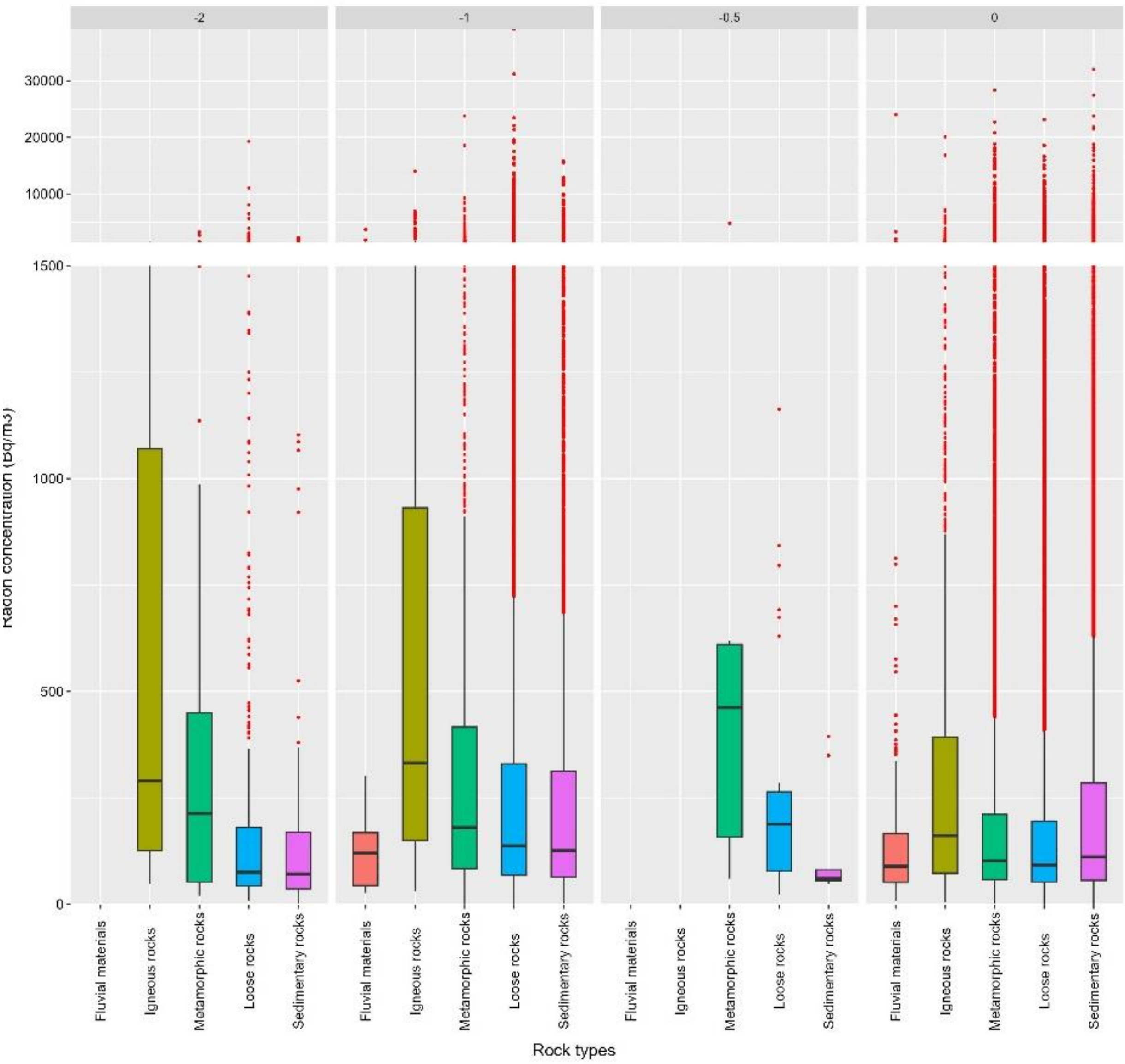

Figure 27 - Boxplot distributions of IRC relative to the underlying rock type and the floor of investigation at the national scale.

Figure 28 illustrates the distribution of indoor radon levels based on rock type and the spatial boundaries of karstic catchments. At first, within karstic catchments, only sedimentary and loose rock formations are observed. Then and notably, IRC measured in sedimentary rocks within karstic areas are higher compared to the national distribution in the same conditions. Overall, this distribution is comparable to that of igneous rock regions, if not slightly higher. Figure 28 clearly highlights the radon issue in karstic areas.

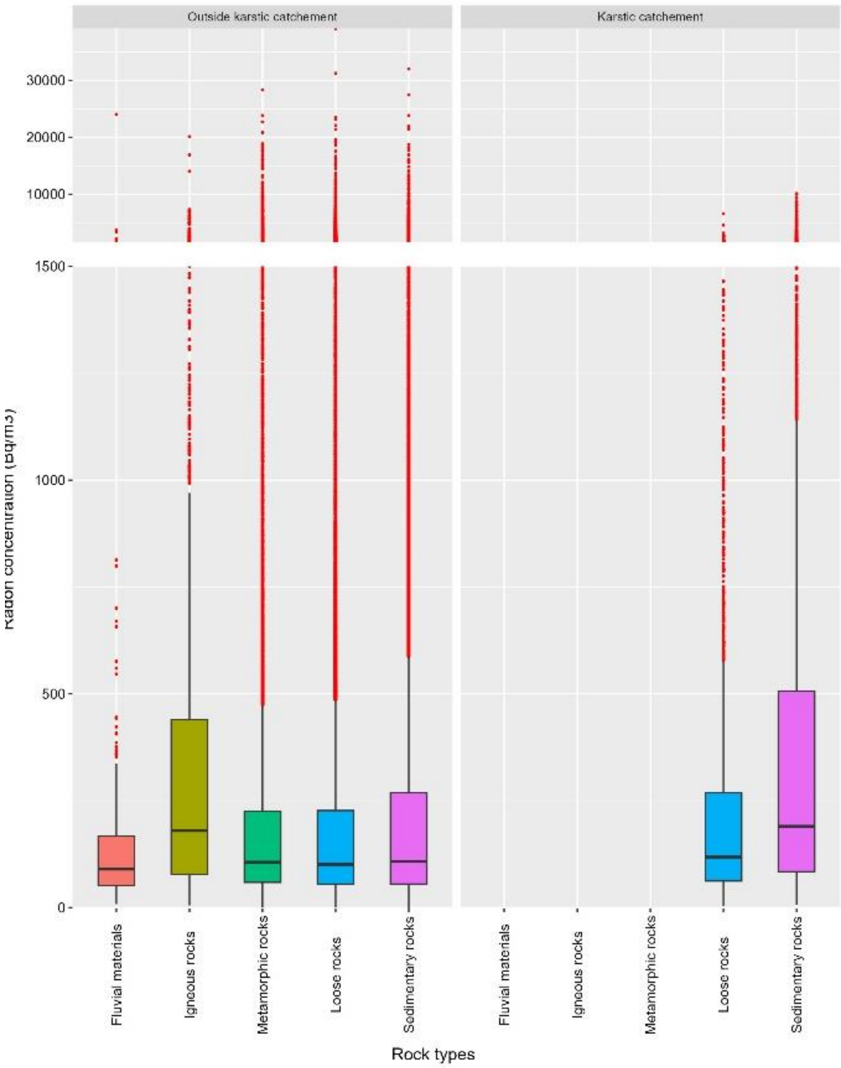

Figure 28 - Boxplot distributions of IRC relative to the underlying rock type at the national scale, and its binary location into a karstic catchment area.

To delve deeper into the analysis, Figure 29 illustrates the relationship between the distance from a fault (tectonic accident) and IRC. When considering all data (at national scale), a clear trend thus emerges. IRC tend to be higher in areas located closer to faults. This observation highlights two key points. Firstly, highly fractured areas are typically found in mountainous regions, which are among the most radon prone areas in Switzerland due to various factors such as building typology, ventilation practices, and heating behaviours. Secondly, these results emphasize the influence of faults on IRC. Faults and karstic voids may enhance air movement within the karstic network and facilitate radon entry into buildings.

Figure 29 does not provide sufficient evidence to distinguish between radon levels in karstic areas and the rest of the country. To further investigate this relationship, Figure 30 presents boxplots that compare IRC across various distance ranges from faults. Additionally, Table 28 summarises the number of observations within each distance range, differentiating between locations situated inside and outside karstic catchments. When analysing the combined data, a consistent trend emerges for most of the distance ranges examined, IRC are significantly higher in karstic areas compared to non-karstic regions. This disparity is particularly evident for distances less than 1 km from faults, where the influence of geological features such as karst voids and fault-related fractures is likely more pronounced. These geological structures may enhance radon mobility and increase its infiltration into buildings located near faults.

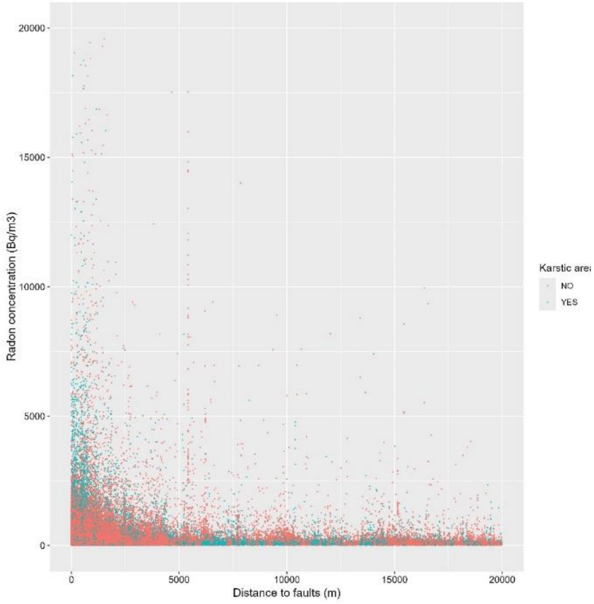

Figure 29 - Distribution of indoor radon measurements relatively to its distance (m) to the closest fault and its binary location into a karstic catchment area

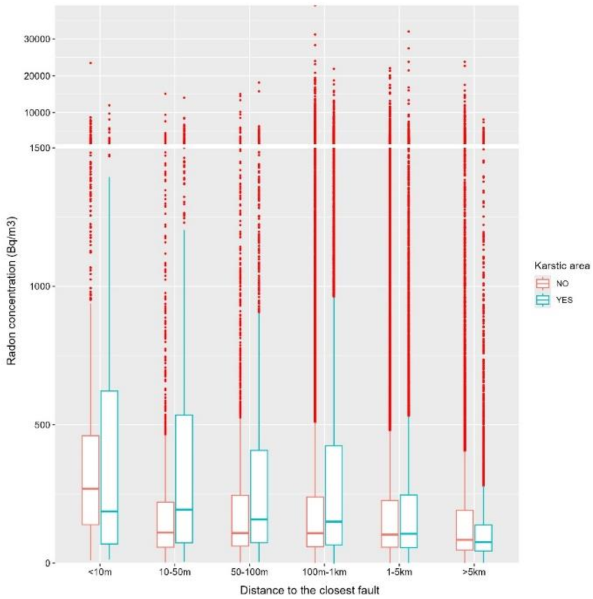

Figure 30 - Boxplot distributions of indoor radon measurements according to distance range to the closest fault and its binary location into a karstic catchment area

Table 28 - Number of indoor radon measurements carried out according to the distance range investigated

	< 10 m	10 – 50m	50 – 100m	100m – 1km	1– 5km	> 5 km
Karstic catchments	226	1043	1485	14033	11624	5896
Outside Karstic catchment	1357	1823	2372	33954	37802	15635

2.5.5 Synthesis and discussion about Swiss application

The analysis conducted in this study provides valuable insights into the relationship between geological features and IRC across Switzerland. Figure 26 demonstrates that the highest radon levels are associated with igneous rocks, such as granitic massifs, followed by sedimentary rocks. These results highlight the importance of rock type as a key determinant of radon accumulation. Expanding on this, Figure 27 underscores the influence of building levels on radon measurements. Higher radon concentrations are consistently observed in igneous rock areas, particularly on ground floors. In contrast, sedimentary and metamorphic rock areas display elevated radon levels respectively in ground floor, and in basements (-1 and -2 levels), reflecting differences in radon infiltration mechanisms and building typologies.

Karstic catchments present a unique challenge, as illustrated in Figure 28. Within these areas, sedimentary rocks are dominant, and radon concentrations are significantly higher than the national averages for similar rock types (*i.e.* sedimentary). This trend aligns closely with radon levels in igneous regions, if not slightly exceeding them. The spatial correlation between karstic networks and elevated radon levels suggests that karstic voids play a critical role in radon mobility and infiltration. Faults and karstic networks, through enhanced air movement and climate-driven processes, may facilitate radon entry into buildings, as suggested in Figure 29 and Figure 30. Additional analysis of distances from faults further reinforces these findings. Radon concentrations are highest within 1 km of faults, particularly in karstic areas, where the combination of geological fractures and voids promotes radon transport. These observations emphasise the double role of geological formations and proximity to faults in shaping radon distribution patterns.

3 Overall description and conclusions

The analyses conducted by different European partners within the RadoNorm project, with the overarching goal of studying the influence of underground voids on radon levels. The work was divided among the partners, each focusing on specific regional contexts and types of voids, thereby contributing to a broader understanding of the phenomenon.

3.1 Austrian Analysis

The Austrian analysis examined IRC in relation to karstificable lithologies, geological faults, and underground voids associated with mining sites, using an extensive Austrian IRC dataset, geological maps, and mining site data. The results indicate that karstificable lithologies show high median IRCs, exceeded only by the crystalline rocks of the Bohemian Massif. No clear overall trend emerged regarding the influence of the distance from geological faults on IRC for all lithologies, although a weak decreasing trend was observed for non-karstificable alpine lithologies at distances less than 100 meters from the faults. Regarding mining sites, the overall effect on IRC was not consistent, with both positive and negative correlations found for individual sites, depending on the type and depth of the mine. However, with the exception of low IRCs very close to the sites (<100 m), a general trend of decreasing IRC with increasing distance was observed for both shallow and deep mining sites. The analysis suggests that underground voids resulting from mining activities could have complex effects on radon levels by altering permeability or acting as radon "reservoirs". Regarding the decrease of IRC with increasing distance to geological faults, the results in Switzerland analysis were much clearer than that in Austria. This of course can have different reasons, as different data sources for the characterisation of geological faults, or different scales of the used data sets for geological faults.

3.2 Czech Analysis

The analysis carried out by the Czech Republic focused on the north-western part of the country, an area characterised by a low geological radon index but with a significant presence of underground voids resulting from mining activities (coal, kaolin, precious metals). Data from more than 170,000 indoor radon measurements in residential and school buildings, collected in the national radon database, were used. The analysis compared two subsets of buildings: those located in non-undermined areas and those partially or entirely located above underground voids. The results suggest that the presence of underground voids may contribute to increased IRC, even in areas that, from a purely geological perspective, would not be considered high-risk. This effect is more evident in houses built directly above mined areas. Although the data show significant variability, the observed trend indicates a possible correlation between the presence of underground voids and elevated radon levels, underlining the importance of considering anthropogenic structures when assessing radon risk.

3.3 French Analysis

The French analysis focuses on an ongoing study in a karstic pilot area in the French Jura mountains. The research aims to understand the mechanisms of radon-222 formation and transfer in karstic environments and their impact on soil radon levels and surface exhalation. Previous geogenic radon potential mapping in France did not specifically account for karstic influences due to their heterogeneity and the lack of data on radon transfer within them. Initial findings in the study area showed a significant enrichment of radium-226 in the soil and elevated indoor radon-222 levels. Strong spatial variability in soil-gas radon concentrations was observed, with karstic structures such as sinkholes and fractures appearing to play a significant role. The study employs *in-situ* measurements, data analysis, and numerical modelling using the T2Rn code.

3.4 Italian Analysis

The Italian analysis, conducted on data from the Municipality of Rome, evaluated the potential correlations between IRC in dwellings and their distance from various types of urban voids. The study used two datasets: one with the locations of over 3000 voids (including bunkers, catacombs, tunnels, etc.) and another with over 1400 IRC measurements from a 2010 survey. The analysis defined concentric rings around the centres of the voids and calculated the mean radon concentration in dwellings within these rings, up to a distance of 100 meters. The main finding is that no significant variations in mean radon concentration were observed in relation to the distance from the void centres. An additional analysis considering the floor level of the dwellings did not yield conclusive results due to limited data for certain categories. The study concludes that no generalised correlation was found between the distance from urban voids in Rome and indoor radon levels in the dwellings above them.

3.5 Swiss Analysis

The Swiss analysis investigated the correlation between radon in underground cavities and indoor radon levels, using a large national database of indoor radon measurements and georeferenced data. The study found that igneous rocks are associated with the highest indoor radon levels nationwide. However, a particularly significant finding concerns karst areas, where radon concentrations measured in sedimentary rocks were considerably higher than the national average for the same rock type, reaching levels comparable to or even exceeding those found in regions with igneous rocks. Furthermore, the analysis revealed a tendency for higher IRC near geological faults, particularly within karst areas, suggesting that these structures may facilitate the transport of the radioactive gas.

This study highlights the complex interactions between geology, karstic features, and radon exposure. The findings confirm that:

1. Igneous rocks, such as granite, pose the highest risk for elevated IRC at the national scale.
2. Karstic areas, particularly those near faults, exhibit disproportionately high radon levels, which are in contrast with radon levels in other sedimentary rocks areas.
3. Proximity to faults is a significant factor, as faults can enhance radon transport and infiltration into buildings, especially in karstic areas.

These results underline the need for targeted radon mitigation efforts, especially in karstic and fault-prone areas. Future studies should further investigate the specific mechanisms of driving radon transport in these regions and consider integrating these findings into public health policies to reduce radon exposure risks.

3.6 Comparison of Results of Collaborative Work

The work of the different partners, although focused on specific contexts, contributes to a more comprehensive understanding of the influence of underground voids on radon levels.

- Switzerland and Austria both highlighted an association between karstic areas and elevated indoor radon levels, suggesting that the common geological characteristics of these regions (permeability, fractures) favour high radon levels. In particular, the Swiss analysis emphasised the role of geological faults in this process, an aspect less evident in the Austrian results. This difference could be due to different data sources on faults or other regional specificities.
- France is conducting an in-depth study on the radon transport mechanisms in a specific karstic area, combining *in-situ* measurements and numerical modelling. This approach aims to provide a more detailed understanding of the processes leading to high radon levels in these environments, complementing the more statistical analyses conducted by other partners.
- Czech Republic observed an increase in radon levels in buildings located above former mining areas, even in zones with a low geological radon index. This suggests that the influence of underground voids can be substantial even in geologically low-risk settings, highlighting the importance of combining geological and infrastructural data when assessing radon exposure.
- Italy, focusing on anthropogenic voids in an urban context, did not find a significant correlation between the distance from these voids and indoor radon levels. This suggests that the impact of voids on radon may strongly depend on the type of void (natural vs. anthropogenic), the geological characteristics of the site, and ventilation mechanisms.

The collaborative work is manifested in the sharing of a common objective (to study the influence of underground voids on radon) and in the application of different methodologies (analysis of existing databases, GIS, correlation studies, modelling) in different geographical and geological contexts. Each partner contributed their expertise and data, allowing for the exploration of the complexity of the phenomenon from different perspectives. The differences in results among the partners, such as the strong association between karst and radon in Switzerland and Austria compared to the lack of correlation with urban voids in Rome, highlight the importance of the specific context and underscore the need to consider various factors when assessing radon risk.

3.7 Conclusion

In conclusion, the analyses of the different partners in the RadoNorm project provide a heterogeneous but complementary picture of the influence of underground voids on radon levels. The comparison of results highlights how the type of void, the geological context, and the analysis methodology are crucial factors in understanding this complex relationship. The joint work allows for more solid conclusions and the identification of priority areas for future research and radon risk mitigation measures.

The sources highlight the complex relationship between underground voids and radon levels, with karstic environments in Switzerland and Austria showing a more pronounced association with elevated radon compared to the urban voids studied in Rome. The influence of geological faults appears significant in the Swiss context, while the impact of mining sites in Austria is more localized and variable. The French study aims to provide a deeper understanding of radon behaviour in karstic systems. The overall picture suggests that the type and geological context of the underground voids, as well as the broader geological characteristics of the region, are crucial factors in determining their influence on surface and indoor radon levels. The case of the Czech Republic, where a measurable impact of anthropogenic voids (abandoned mines) on indoor radon levels was observed despite the absence of favourable geological conditions, highlights the importance of including both geological and anthropogenic parameters in future radon risk mapping. This multidimensional approach is essential for improving mitigation strategies and better protecting citizens exposed to radon risk across Europe.

4 References

1. Somlai, J. et al. 2006. *Radon concentration in houses over a closed Hungarian uranium mine.* Sci Total Environ, 367(2-3): 653-665.
2. Magrini, A.G.M. et al. 2007. *Analysis of the natural radioactivity due to the radon gas in the underground of Rome; [Analisi della radioattività naturale dovuta al gas radon presente negli ambienti sotterranei della metropolitana di Roma].* Giornale Italiano di Medicina del Lavoro ed Ergonomia, 789-792.
3. Yoshimura, E.M. et al. 2015. *Radon concentration in air and external gamma dose rate: is there a correlation?* J Radioanal Nucl Chem, 307(1): 787-792.
4. Vaupotic, J. 2008. *Levels of nanosize radon decay products in indoor air: a comparison for different environments*. Coll Antropol, 32 Suppl 2: 99-104.
5. Bruzzone, D. et al. 2006. *Measurement of the concentration of radon gas in the Toirano's Caves (Liguria).* Annali Di Chimica, 96(9-10): 515-524.
6. Li, X. et al. 2010. *The distribution of radon in tunnels with different geological characteristics in China.* J Environ Radioact, 101(5): 345-348.
7. Cucos Dinu, A. et al. 2017. *Radon levels in Romanian caves: an occupational exposure survey.* Environ Geochem Health, 39(5): 1085-1099.
8. Sainz, C. et al. 2018. *Continuous monitoring of radon gas as a tool to understand air dynamics in the cave of Altamira (Cantabria, Spain).* Sci Total Environ, 624: 416-423.
9. Rizo-Maestre, C. and Echarri-Iribarren, V. 2020. *Radon Gas in the City of Alicante. High Risk of Low Indoor Air Quality in Poorly Ventilated Buildings.* Int J Environ Res Public Health, 17(23).
10. Zhuo, W. et al. 2000. *Environmental radon and thoron progeny concentrations in Fujian Province of China.* Radiat Prot Dosim, 87(2): 137-140.
11. Leonardi, F. et al. 2021. *Radon Spatial Variations in University's Buildings Located in an Italian Karst Region.* Atmosphere, 12(8).
12. Banrion, M.H. et al. 2022. *Using geogenic radon potential to assess radon priority area designation, a case study around Castleisland, Co. Kerry, Ireland.* J Environ Radioact, 251-252: 106956.
13. Medici, F. and Rybach, L. 1994. *Measurements of Indoor Radon Concentrations and Assessment of Radiation Exposure.* J Appl Geophys, 31(1-4): 153-163.
14. Gasiūnas, K. et al. A. 2012. *Concentrations of Indoor and Soil Radon in Lithuania.* Statyba, 4(4): 316-321.
15. Vaupotic, J. et al. 2000. *Systematic indoor radon and gamma-ray measurements in Slovenian schools.* Health Phys, 78(5): 559-562.
16. Annanmaki, M. and Oksanen E. 1992. *Radon in the Helsinki Metro.* Radiat Prot Dosim, 45(1-4): 179-181.
17. Deb, A. et al. 2016. *Exposure to underground radon in and around Kolkata Municipal Corporation area: an exhaustive study.* J Radioanal Nucl Chem, 311(1): 375-384.
18. Doi, M. and Kobayashi S. 1996. *Surveys of concentration of radon isotopes in indoor and outdoor air in Japan.* Environ Int, 22: S649-S655.
19. Fijalkowska-Lichwa, L. and Przylibski T.A. 2021. *Assessment of occupational exposure from radon in the newly formed underground tourist route under Ksiaz castle, Poland.* Radiat Environ Biophys, 60(2): 329-345.
20. Fijałkowska-Lichwa, L. and Przylibski T.A. 2011. *Short-term ^{222}Rn activity concentration changes in underground spaces with limited air exchange with the atmosphere.* Nat Hazards Earth Syst Sci, 11(4): 1179-1188.
21. Hwang, S.H. et al. 2018. *Radon and NO_2 levels and related environmental factors in 100 underground subway platforms over two-year period.* J Environ Radioact, 181: 102-108.
22. Hwang, S.H. and Park, W.M. 2018. *Radon and PM(10) concentrations in underground parking lots and subway stations with health risks in South Korea.* Environ Sci Pollut Res Int, 25(35): 35242-35248.

23. Kim, D. et al. 2022. *Spatial modeling for radon concentrations in subway stations in Seoul, Korea.* Environ Sci Process Impacts, 24(1): 116-126.
24. Kim, D.S. and Kim, Y.S. 1993. *Distributions of airborne radon concentrations in Seoul metropolitan subway stations.* Health Phys, 65(1): 12-16.
25. Liendo, J. et al. 1997. *Radon monitoring for health studies in the Caracas subway using SSNTDs.* Radiat Meas, 28(1-6): 729-732.
26. Long, S.C. et al. 2016. *Factors underlying persistently high radon levels in a house located in a karst limestone region of Ireland - lessons learned about remediation.* Nukleonika, 61(3): 327-332.
27. Lu, X. et al. 2008. *An Environmental Risk Assessment of Radon in Lantian Karst Cave of Shaanxi, China.* Water, Air, Soil Pollut, 198(1-4): 307-316.
28. Sabol, J. 1995. *Evaluation of radon concentrations in air and gamma dose rates in the Prague Metro.* Environmental Monitoring and Hazardous Waste Site Remediation, 2504: 409-415.
29. Sajo-Bohus, L. et al. 1997. *Radon concentration measurements in Venezuelan caves using SSNTDs.* Radiat Meas, 28(1-6): 725-728.
30. Song, M.H. et al. 2011. *Radon exposure assessment for underground workers: a case of Seoul Subway Police officers in Korea.* Radiat Prot Dosim, 147(3): 401-405.
31. Talaeepour, M. et al. 2006. *Investigation on Radon Concentration in the Tehran Subway Stations, in Regard with Environmental Effects.* J Appl Sci, **6**(7): 1617-1620.
32. Tan, B. et al. 2020. *Study On Radon Concentration Variation During Subway Construction.* Radiat Prot Dosim, 191(4): 409–422.
33. Vaupotič, J. et al. 2017. *Radon dynamics in a dwelling with high radon levels in a karst area.* Geological Society, London, Special Publications, 451(1): 63-82.
34. Xue, X.W.Z. et al. 2020. *Survey and Assessment of Radon Concentration in Guiyang Metro Line 1.* Nuclear Electronics and Detection Technology, 40(4): 681-684.
35. Yafasov, A.Y. and Akimov, V.A. 2001. *Systematic indoor radon and gamma-ray measurements in Slovenian schools.* Atomic Energy, 90(2): 130-136.
36. Yoon, S. et al. 2010. *Indoor radon distribution of subway stations in a Korean major city.* J Environ Radioact, 101(4): 304-308.
37. Yu, K.N. et al. 1996. *A survey of radon properties in underground railway stations in Hong Kong.* J Radiol Prot, 16(1): 37-43.
38. Gruber, V. et al. 2021. *The new Austrian indoor radon survey (ÖNRAP 2, 2013–2019): Design, implementation, results*. J Environ Radioact, 233: 106618.
39. Geologische, B. 2020. Geological map of Austria, 1:500 000, Data Set KM500 Austria. https://www.geologie.ac.at/en/research-development/mapping/geology.
40. Iris, Interaktives Rohstoffsystem. https://www.geologie.ac.at/services/webapplikationen/iris-interaktives-rohstoffinformationssystem
41. Ielsch, G. et al. 2010. *Mapping of the geogenic radon potential in France to improve radon risk management: methodology and first application to region Bourgogne.* J Environ Radioact, 101: 813-820.
42. Von Gunten, H.R. et al. 1996. *Uranium Series Disequilibrium and High Thorium and Radium Enrichments in Karst Formations.* Environ Sci Technol, 30(4).
43. Cholet, C. 2017. Fonctionnement hydrogéologique et processus de transport dans les aquifères karstiques du Massif du Jura. Université de Franche-Comté.
44. Neznal, M. 2005. *Permeability as an important parameter for radon risk classification of foundation soils.* Ann Geophys, 48(1): 175-180.
45. Girault, F. and Perrier F. 2012. *Measuring effective radium concentration with large numbers of samples. Part I – experimental method and uncertainties.* J Environ Radioact, 113: 177-188.
46. Columbu, S. et al. 2021. *Strategies for helium pycnometry density measurements of welded ignimbritic rocks.* Measurement, 173: 108640.
47. Saâdi, Z. et al. 2014. *EOS7Rn—A New TOUGH2 module for simulating radon emanation and transport in the subsurface.* Comput and Geosci, 65: 72-83.
48. Swiss Federal Office of Public Health, 2020. *National Action Plan concerning Radon 2021 – 2030.* Federal Office of Public Health.
49. Swiss Federal Office of Public Health, 2017. *Carte radon [Grid].* FOPH. https://www.geocat.ch/geonetwork/srv/eng/md.viewer#/full_view/54a8a239-ace3-4510-8fd4-7b4ddc370727/tab/complete

50. Rey, J. 2024. *Assessment of methods for radon detection in buildings.* EPFL, Lausanne. https://doi.org/10.5075/EPFL-THESIS-11093
51. Office fédéral de topographie suisse, 2014. *GéoCartes500.* swisstopo, Bern.
52. Reusser, J.E. et al. 2023. *Geochemical Soil Atlas of Switzerland: Distribution of 20 elements in the topsoil.* Agroscope. https://doi.org/10.34776/gca23-e
53. Reusser, J.E. et al. 2023. *Geochemical Soil Atlas of Switzerland - Distribution of Toxic Elements.* Chimia, 77(11): 758-763.
54. Office fédéral de l'environnement, OFEV, *Informations pour spécialistes: Tremblements de terre.* https://www.bafu.admin.ch/bafu/fr/home/themen/thema-naturgefahren/fachinformationen-erdbeben.html
55. Frehner, M. et al. 2005. *Gestion durable des forêts de protection. Soins sylvicoles et contrôle des résultats: instructions pratiques. (L'environnement pratique).* Office fédéral de l'environnement, des forêts et du paysage, 564 p
56. MétéoSuisse, Cartes des normales saisonnières. https://www.meteosuisse.admin.ch/climat/climat-de-la-suisse/normes-climatologiques/cartes-des-normales-saisonnieres.html
57. Bundesamt für Umwelt, B., Nationale Grundwasserbeobachtung NAQUA. https://www.bafu.admin.ch/bafu/de/home/themen/wasser/fachinformationen/zustand-der-gewaesser/zustand-des-grundwassers/nationale-grundwasserbeobachtung-naqua.html